ADVANCED FUNCTIONAL MATERIALS

www.afm-journal.de

Check for updates

# Silicon-Compatible Photodetectors: Trends to Monolithically Integrate Photosensors with Chip Technology

*Wei Yang, Jiaxin Chen, Yong Zhang, Yujia Zhang, Jr-Hau He,* and Xiaosheng Fang**

**Encouraged by the increasing requirements of intelligent equipment, silicon integrated circuit–compatible photodetectors that support single-chip photonic–electronic systems have gained considerable progresses. Advanced materials have resulted in enhanced device performance based on traditional photovoltaic effect and photoconductive effect, and novel device designs have catalyzed new working mechanisms combing rapid photoresponse and high responsivity gain. Surprising applications are developed using monolithic photonic–electronic platforms, and the developing integration strategies keep pace with the developing complementary metal-oxide-semiconductor techniques as well as nonsilicon substrates. Here, the recent developments in silicon-compatible photodetectors, both in device advances and their integration routes, are reviewed. Meanwhile, the progresses, challenges, and possible future directions in this field are discussed and concluded.**

## 1. Introduction

Thanks to the development of "Internet of Things" (IoT) and intelligent devices, our lives have been obviously facilitated in the past few years. Machines and devices are becoming more and more smart with the help of artificial intelligence and various sensors, and an exciting glimpse of a bright future has been caught. As one of the most important type of sensors, photodetectors that can precisely convert incident light into electrical signal have been attracting increasing attention. Vast applications including photosensors, spectral analysis, environment monitoring, communication, imaging and so on have been realized based on narrowband or broadband photodetectors from ultraviolet to terahertz.[1] Traditionally, "5S" requirements are used to evaluate a photodetector, namely, stability, signal-to-noise (STN) ratio, sensitivity, speed, and selectivity, which attract more attention among other properties in the past.[2] However, the boosting advances of miniaturized intelligent devices are expecting novel photodetectors with additional compatibility to integrated circuits to provide advanced functions like logic analysis.[3]

Although numerous semiconducting materials have been studied in the past few decades, silicon is still the most important material with the widest applications. Abundant silica resources guarantee large-scale silicon production and contribute to low price. Besides its excellent resistance to thermal and oxygen, silicon has goodish carrier mobility of 1350 $cm^2 V^{-1} s^{-1}$ and 480 $cm^2 V^{-1} s^{-1}$ for electrons and holes, respectively. Controlled doping and epitaxial growth have catalyzed mature chip technologies like complementary metal-oxide-semiconductor (CMOS), which generate powerful silicon integrated circuits (silicon-ICs) that form the foundation of smart devices. As demonstrated in **Figure 1**a, traditional photodetectors need additional electronic components to get integrated with silicon-ICs and have troubles in forming miniaturized smart equipment,[4] which only fits normal applications. However, silicon-IC-compatible or silicon-compatible photodetectors can monolithically integrate silicon electronics with optical components. This enables single-chip photonic–electronic systems with intrinsic logic calculations, memory function, and interconnections (Figure 1b), which is getting increasingly important nowadays.

There has been enough theoretical background for the long-term stable operation of photosensors based on silicon. Massive silicon-based photodetectors have been reported owing to the abundant reserves, high photovoltaic efficiency, and mature processing technology.[5] However, only some of them could be considered compatible with the current chip fabrication. The bulk CMOS chips still dominate the modern chip industry, and silicon-IC-compatible devices need to be constructed on bulk silicon wafer rather than nanostructured silicon materials in order to get full benefit from the silicon chip industry.

Mature p- or n-type doping generates different bulk silicon materials with tunable electrical properties, which have strongly facilitated the material choosing in bulk silicon–based photodiodes. Thus, plenty of bulk silicon–based photodiodes have been achieved with silicon or additional heterogeneous nonsilicon materials. Commercial silicon p–i–n photodiode is currently the most widely used photosensors for photoimaging and spectral analysis, not to mention the advanced

W. Yang, J. Chen, Y. Zhang, Dr. Y. Zhang, Prof. X. S. Fang
Department of Materials Science
Fudan University
Shanghai 200433, P. R. China
E-mail: xshfang@fudan.edu.cn

Prof. J.-H. He
Computer, Electrical and Mathematical Sciences and Engineering (CEMSE) Division
King Abdullah University of Science and Technology (KAUST)
Thuwal 23955-6900, Kingdom of Saudi Arabia
E-mail: jrhau.he@kaust.edu.sa

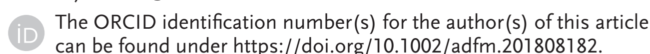
The ORCID identification number(s) for the author(s) of this article can be found under https://doi.org/10.1002/adfm.201808182.

**DOI: 10.1002/adfm.201808182**



© 2019 WILEY-VCH Verlag GmbH & Co. KGaA, Weinheim

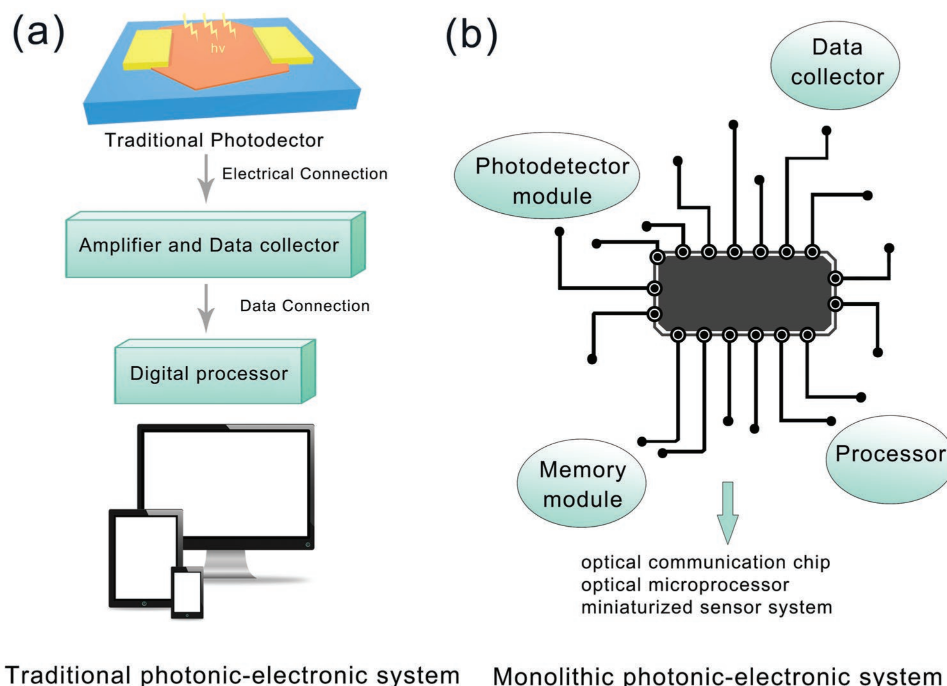


**Figure 1.** Schematic diagrams of a) the typical photonic–electronic system based on traditional photodetectors and b) the monolithic photonic–electronic system based on silicon-IC-compatible photodetectors.

photodiodes with improved performance. The epitaxial dielectric or semiconducting layer also plays an important role in the device architecture. For example, surface-oxidized silicon wafers realize vertical insulation and contribute to gate-tunable photodetectors like photo-field-effect transistors (photo-FETs). These merits immensely enrich the device structures and the material candidates, offering huge potentials to develop high-performance silicon-compatible photodetectors.

However, silicon materials also suffer obvious shortcomings in photosensitivity. The indirect bandgap of silicon makes it an insufficient photoconductive material, and the bandgap of 1.1 eV results in an absorption decrease beyond 800 nm with a typical photosensitive cutoff at 1100 nm. Therefore, silicon is not considered as an ideal photosensitive material, especially beyond the short-wavelength near-infrared (SW-NIR) region. The widely used visible light detection prefers a moderate device bandgap of around 1.7 eV while UV detection requires even larger bandgaps, where silicon materials are less photosensitive and introduce IR noise. It is still of great importance to solve these problems and pursue higher performance enhancement for silicon-compatible photosensors.

Plenty of progresses have been reported in this field over the past decade, both in photodetectors and the integration strategy with silicon-ICs. Various surface modifications and mid-bandgap absorption in silicon materials have effectively enhanced the spectral response beyond 1100 nm, expanding the application range of silicon-based photodetectors. A lot of novel materials were utilized to form photosensors with silicon and effectively modulated the spectral response in the UV-to-NIR region. Also, the rapid development of new materials like 2D materials[6] has greatly enriched the candidate materials of silicon-based van der Waals (vdW) heterojunction and successfully resulted in exciting multilayered device structures with outstanding photosensitive properties.[7] As for the integration studies, former researches have reported many successful monolithic photonic–electronic platforms based on early silicon-compatible photodetectors, enabling advanced applications in high-fidelity light communications chips,[8] high-bandwidth light processor and memory chips,[9] and highly parallel photobiochemical sensors.[10]

This review covers the basic description and recent progresses of silicon-compatible photodetectors and the integration methods into silicon chips. We begin by offering a brief introduction about photodetectors. Then, we fully describe the advances in silicon-compatible photodetectors with traditional working mechanisms (photovoltaic effect and photoconductive effect) and a novel mechanism. The widely used photovoltaic-type architecture still shows huge potential in high-speed bulk silicon–based photodetectors. Some important progresses have been achieved for high-detectivity silicon-compatible photoconductive devices. Moreover, recent novel working mechanism of the photovoltage and transconductance gain has been proposed to simultaneously realize high responsivity gain and ultrafast photoresponse. After that, the developments of the integration strategies are demonstrated to prepare single-chip photonic–electronic systems. Finally, we conclude the challenges and discuss the exciting avenues enabled by material advances and device designs.

## 2. Information about Photodetectors

Typically, photodetectors are constructed on the basis of photovoltaic effects or photoconductive effects. Photovoltaic effects are based on built-in electric fields, where photogenerated


© 2019 WILEY-VCH Verlag GmbH & Co. KGaA, Weinheim

carriers are separated and even drifted to form photocurrent. Photovoltaic devices or photodiodes can be classified as homojunction photodiodes, heterojunction photodiodes, and Schottky photodiodes according to their junction types. Photoconductive effects originate from the increased conductivity of semiconductors under illumination. The incident light generates photoinduced carriers and contributes to extra photoconductivity when the photon energy is above the bandgap of semiconducting materials. Metal–semiconductor–metal (MSM) device and photo-FET are typical photoconductive devices. Recently, the photovoltage and transconductance gain has been realized using commercial silicon processing, which was reported with remarkable device performances (as stated in Section 5). The main parameters of photodetectors are described as follows:

The photoelectric conversion ability is often evaluated by responsivity $R$, which is directly defined as the ratio of photocurrent $I_{ph}$ to the incident light power $P_{in}$. $R$ is actually determined by the external quantum efficiency (EQE, i.e., numbers of effective electron–hole (e–h) pairs generated per incident photon, determined by the light absorption and charge separation efficiency) and gain ratio $G$ (numbers of carriers detected per photogenerated e–h pair). The relationships among these parameters are displayed as follows

$$R(\mathrm{AW}) = \frac{I_{\mathrm{ph}}}{P_{\mathrm{in}}} = \mathrm{EQE}\frac{q\lambda}{hc}G \tag{1}$$

where $q$ refers to electron charge, $h$ is the Planck constant, $\lambda$ is the incident wavelength, and $c$ is the speed of light.

The sensitivity can be described as the ability to distinguish weak incident signal. The signal-to-noise ratio represents the sensitivity of a photodetector, which is defined in Equation (2)

$$\text{signal-to-noise ratio} = \frac{I_{\mathrm{ph}}}{I_{\mathrm{N}}} \tag{2}$$

The noise current $I_N$ should comprise all noise sources in a photodetector, but only the short noise current $I_{SN} = (2qI_{dark})^{1/2}$ is often considered in the calculation. Thermal noise (Johnson–Nyquist noise) is also considerable, and flicker noise cannot be neglected under low on–off frequency (typically <500 Hz). Compared to STN, the lowest detectable power or the noise-equivalent power (NEP) is more intuitive to evaluate a photodetector. NEP is defined as the incident light power when STN = 1. However, NEP depends on different device parameters such as device area $A$ and device bandwidth $B$. In order to facilely evaluate photodetectors with different bandwidths and sizes, specific detectivity $D^*$ has been introduced according to Equation (3)

$$D^*\left(\mathrm{cm\ Hz^{-1/2}W^{-1} = Jones}\right) = \frac{\sqrt{AB}}{\mathrm{NEP}} = \frac{R\sqrt{AB}}{I_{\mathrm{N}}} \tag{3}$$

Response speed is attracting increasing attention due to the increasing high-frequency requirements in autonavigation and instant interaction. The response time, including rise time $\tau_r$ and fall time $\tau_f$, is defined as

$$\text{response time}(\tau_r, \tau_f)(\mathrm{s}) = |t_{90\%} - t_{10\%}| \tag{4}$$

where $t_{90\%}$ and $t_{10\%}$ refer to the time to reach 90% and 10% of the photocurrent, respectively.

High-selective photodetectors is crucial for many applications such as machine vision, intelligent surveillance, and color photography,[11] and color selectivity is evaluated by the half-bandwidth in the responsivity–wavelength curves.

Silicon-compatible photodetectors have advantages in developing smart photosensors, which may lead novel photosensors in advanced applications like IoT photosensors.[12] Apart from the above-mentioned traditional "5S" requirements, additional "3S" requirements (smart, small, and energy saving) are pursued in IoT photosensors.

1. *Smart (data-processing ability)*: Simple photosensors are only endowed with the core function to collect light signal and generate electric data, while IoT applications prefer smart photosensors with additional logic functions. Therefore, both data processing and data transmission should be realized apart from the core photoelectric properties to get the compatibility with IoT networks. Here, silicon-compatible devices enable facile single-chip photonic–electronic for facilitated and miniaturized data processing and data transmission.
2. *Small (low space occupation)*: Considering the specific working condition, physical space is usually highly limited in IoT devices and small photosensors are desired. Here, small photosensors not only refer to the miniaturized photodetectors but also include the avoidance or miniaturization of supporting components such as power sources, current amplifiers, data processors, memorizers, connectivity parts, etc. Thus, properties such as high photocurrent (avoid current amplifiers), self-power (avoid power sources), and silicon-compatibility (miniaturize the electronic components and the connectivity parts) have become more important in IoT photosensors
3. *Energy saving (self-power or low power consumption)*: The limited installation space and the ubiquitous requirements make IoT photosensors unable to rely on bulk power sources. IoT photosensors have to keep a perennial performance with small batteries or in a self-powered mode to reduce the maintenance frequency.

## 3. Silicon-Compatible Photovoltaic Photodetectors

### 3.1. Advances in Traditional Silicon Photovoltaic Devices

Due to the different Fermi energy levels, free carriers spontaneously diffuse to the counterparts near the homointerface, heterointerface, and Schottky semiconductor/metal interface, forming depletion region (or space charge region) in photovoltaic devices.[13] Subsequently, the remained charge centers generate built-in electric field and suppress leakage current. The built-in electric field helps to separate photoinduced e–h pairs in the depletion region and contribute to enhanced photocurrent. The charge separation process is much faster than carrier diffusion process, thus fully depleted photovoltaic photodetector shows obvious advantages in high response speed.

The widely used commercial silicon photovoltaic devices are based on silicon homojunctions.[14] Thanks to the excellent lattice match, homojunction photodiodes show excellent stability even in extreme working conditions. Doping introduces little lattice deformation and the lattice-matched homojunction


© 2019 WILEY-VCH Verlag GmbH & Co. KGaA, Weinheim

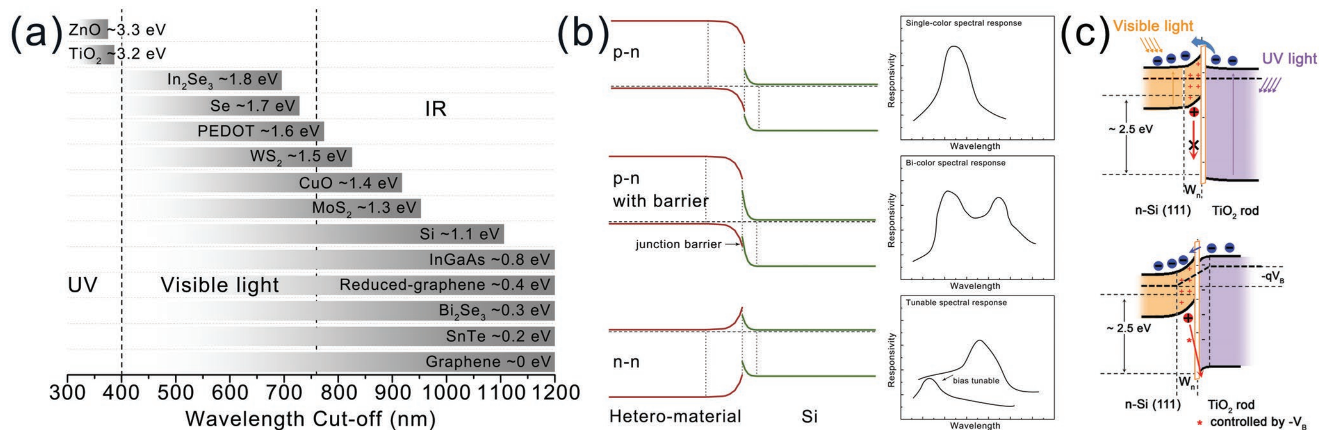


**Figure 2.** a) The photosensitive materials in recent silicon-compatible photodiodes with bandgaps ranging from UV to IR regions. b) Description of the typical relationship between the energy band structure and the spectral response. c) The bias-tunable spectral response taking the n-Si(111)/$TiO_2$ multicolor photodiode as an example. Reproduced with permission.[17a] Copyright 2016, Wiley-VCH.

interface guarantees highly uniform built-in electric field. So, commercial silicon p–i–n photodiode is endowed with goodish photosensitive properties.[15] However, silicon homojunction photodiodes directly inherit the photoelectric properties of silicon materials. They are unsensitive to longer-wavelength light and poorly sensitive to UV light.

Forming heterojunctions offers a facile route to adjust the spectral response of silicon-compatible photodiodes. Various semiconductor materials with different electrical and optical parameters can provide enough flexibility for the design of photoelectric devices, and the easily controlled doping in silicon further enriches the energy band match. As showed in **Figure 2**a, the spectral response of silicon-based heterojunction photodetectors has been expanded to the UV-to-LWNIR (long-wavelength NIR) region based on various materials with different bandgaps, including n-ZnO,[16] $TiO_2$,[17] γ-$In_2Se_3$,[18] Se,[19] InGaAs,[20] PEDOT:PSS,[21] CuO,[22] p-$WS_2$,[23] $MoS_2$,[24] SnTe,[25] $Bi_2Se_3$,[26] reduced graphene oxide,[27] and graphene.[28] However, the spectral response depends not only on the bandgap of the semiconductor material but also on the energy band structure of the junction. The energy band structures of heterojunctions are more complicated compared to that of homojunctions, where junction barrier and type-I energy band match possibly exist.[29] This offers additional flexibility for the spectral response besides the heterogeneous materials. Figure 2b displays the relationship between the energy band structure and the spectral response. The heterojunction photodiode delivers a single-peak spectral response in a finely matched type-II p–n heterojunction, where the junction barrier is avoided and possible antibarrier is formed (the first situation in Figure 2b). In this case, the heterojunction individually confines holes and electrons to the two materials, and the photogenerated carriers are facilely separated and drifted to the two electrodes when the incident photon energy is above the bandgaps of two materials. When the incident wavelength is between the two bandgaps, only the lower-bandgap material can generate photoinduced carriers and no more photoinduced carriers are generated in the other side. The photoexcited charges drift to larger-bandgap side but few drift back to keep an electric neutrality, resulting in a thorough wavelength cutoff corresponding to the larger bandgap. The individual carrier confinement can be disturbed by the junction barrier (the second situation in Figure 2b), and the larger-bandgap wavelength cutoff is weakened then. Thereby bicolor or broadband photoresponse is formed above the lower bandgap. Moreover, an interesting bias-tunable spectral response is sometimes generated under high junction barrier (the last situation in Figure 2b), which is also observed in some silicon-based photodiodes.[17a,30] Here we take Hu and co-workers' work as an example (Figure 2c).[17a] In their n-Si(111)/$TiO_2$ type-I n–n heterojunction, the energy barrier and the band energy difference naturally prevent the carrier transportation across the junction interface. The energy level of the photoinduced carriers is determined by the wavelength of the absorbed incident light. The high-energy UV-induced carriers from the $TiO_2$ side can get across the junction energy barrier while the low-energy photocarriers in the silicon side are trapped, delivering a UV photosensitivity under small bias. Under high reverse bias, the $TiO_2$ energy band is lifted above the band bending of silicon and the visible light detection is switched on. In this way, the n-Si(111)/$TiO_2$ device is enabled with bias-controllable spectral photoresponse.

Apart from adjusting the photosensitive wavelength range of silicon materials, the nanostructured composite materials may also introduce extra property enhancement due to additional mechanisms besides photovoltaic effect. **Figure 3**a displays a silicon-compatible heterojunction photovoltaic photodetector based on p-Si/n-ZnO heterojunction.[16a] Wide-bandgap materials like ZnO strengthen the UV absorption and improve the photoresponse to UV light. The nanoarray structure plays a very important role here. The increased UV photoresponse is partially ascribed to the enhanced signal absorption by antireflection effects[31] or light trapping.[32] Moreover, the 1D array morphology endows light-self-induced pyro-phototronic effect[33] to further improve the device performances. The incident UV illumination rapidly induces a temperature increase within ZnO nanorods and generates negative pyro-polarization charges at both ends of the nanowire, leading to a distribution of pyroelectric potentials along ZnO crystals. The conduction and valance bands of ZnO increase at the p–n interface,[34] and the carrier mobility is highly enhanced to achieve a high output current.


© 2019 WILEY-VCH Verlag GmbH & Co. KGaA, Weinheim

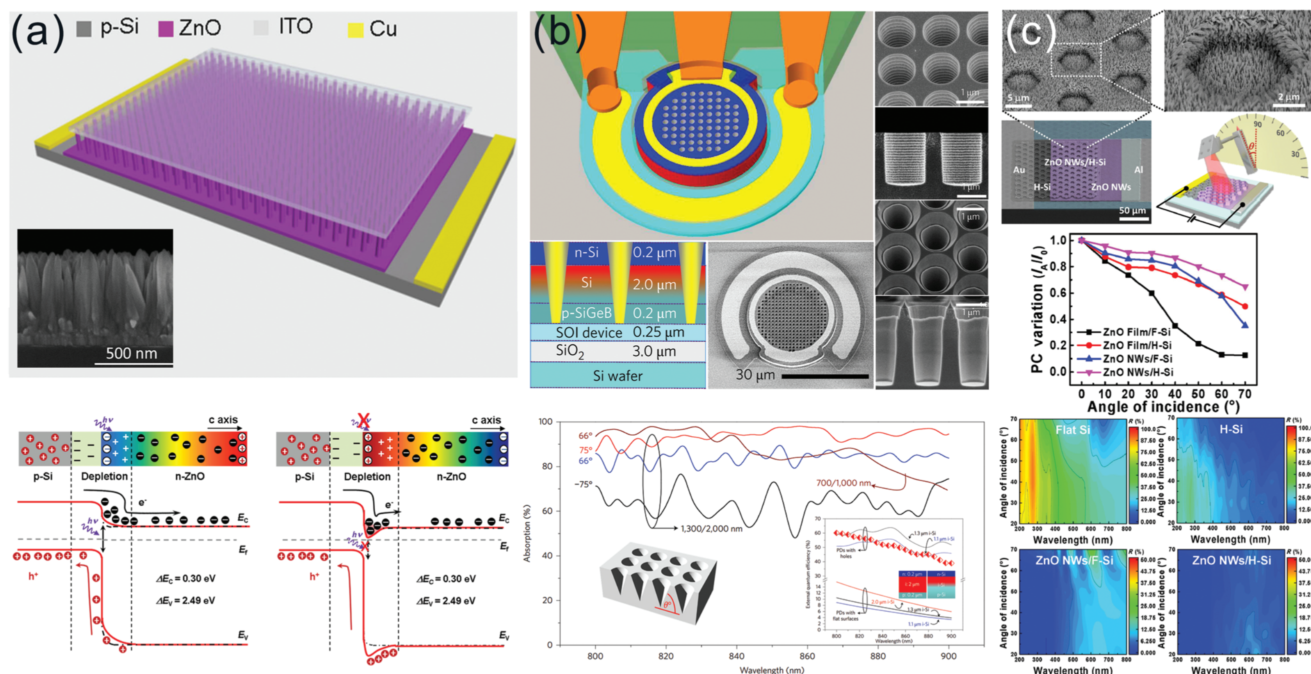


**Figure 3.** Advanced silicon-compatible photodiodes benefiting from nanostructured strategies: a) Silicon-compatible heterojunction photovoltaic photodetector based on p-Si/n-ZnO heterojunction and the light-self-induced pyro-phototronic effect. Reproduced with permission.[16a] Copyright 2016, Wiley-VCH. b) Surface engineering on silicon p–i–n photodiode for high-efficiency light trapping. Reproduced with permission.[35] Copyright 2017, Springer Nature. c) Silicon-compatible broadband omnidirectional photodetector based on interface engineered Si/ZnO heterojunction. Reproduced with permission.[16b] Copyright 2017, Springer.

After the UV illumination turned off, the temperature within ZnO crystals decreases soon and positive pyro-polarization is created. The conduction and valance bands of ZnO decrease and form a carrier trap. Thus, the carrier transportation is severely suppressed, contributing to a low leakage current. In this way, Wang and co-workers achieved a high-performance silicon-compatible photosensor under small bias, which delivered ultrafast photoresponse ($\tau_r/\tau_f$ = 19 μs/22 μs at 325 nm; $\tau_r/\tau_f$ = 15 μs/12 μs at 442 nm) and enhanced responsivity. The response time could be further promoted as the illumination power intensity increases, making it potential for ultrafast strong light detection.

In addition to the various nanostructured nonsilicon materials, the surface engineering of silicon materials also shows huge potential in promoting device properties. Surface nanostructures or microstructures on silicon are often endowed with enhanced light absorption by increasing the absorption area. The light trapping structures can further improve the photoelectric properties and generate high-efficiency silicon-compatible device. In Islam and co-workers' research,[35] microscale and nanoscale holes with different shapes were introduced to silicon p–i–n photodiode to achieve high-efficiency light trapping. As shown in Figure 3b, tapered or cylindrical holes were formed on silicon p–i–n photodiode by patterned reactive ion etch or deep reactive ion etch, respectively. The light trapping strongly improves the light absorption and benefits the photosensitive properties. These surface-engineered silicon p–i–n photodiodes delivered an ultrafast impulse response of 30 ps with a high external efficiency of more than 50%, which is much higher than that in flat silicon photodiodes (lower than 16% at the best result). The taper angle of these holes was tailored by adjusting the isotropic etching and deposition process and obviously influenced the light trapping effect. The morphology optimization of the introduced holes could further improve the external efficiency to more than 70%. Compared to the patterned surface ion etching, forming black silicon is a much cheaper way to increase the light absorption area of silicon wafer. Plenty of researches have been reported on solution-processed black silicon for photoelectric applications.[36] However, black silicon has drawbacks in the traditional device structure of p–n homojunction. The extremely nanostructured surface in black silicon severely increases carrier combinations and limits the device efficiency. In order to make full use of the absorption gain, novel structures with stronger built-in electric field are in demand for charge separation. Using conformal atomic layer deposited alumina was reported as effective route to decrease the surface recombination in black silicon.[37] Recently, Savin and co-workers deposited alumina to construct a conformal layer around the active black silicon area.[38] Thus, an inversion layer was formed and generated a collecting junction with a deep depletion region of 30 μm into the n-type silicon. Such a depletion depth can provide a very high resistivity of more than 10 kΩ cm and the surface recombination is strongly suppressed due to the built-in electric field. Similarly, a uniform alumina layer was fabricated on the bottom side of n-type silicon. The intrinsic high negative surface charge[39] of bottom alumina layer generates a uniform induced junction to avoid the increased dopant-induced recombination inside black silicon, which typically comes from the severely irregular dopant diffusion in silicon nanostructures. Therefore, the


© 2019 WILEY-VCH Verlag GmbH & Co. KGaA, Weinheim

device achieved a remarkable EQE of above 96% from 250 to 950 nm.

Surface-engineered silicon materials also serve as excellent substrates to construct heterojunctions and adjust the device bandwidth. The built-in electric field near the heterojunction interface effectively facilitates the charge separation of the photoinduced carriers and generates many high-performance silicon-compatible devices.[21,22] Moreover, the surface nanostructures not only enhance the light absorption but also contribute to novel applications like omnidirectional photodetection. This has been widely proved in animal eyes and has inspired some biomimetic image sensors that imitate human eye and arthropod eye with microlens arrays.[40] Apart from the microlens arrays, an increasing number of structure designs have been suggested for omnidirectional light harvesting, including nanopencils,[41] inverted nanocones,[42] antireflective multilayer coatings[43] hemispherical geometry,[44] and hierarchical structures.[45] Inspired by these structure designs, Ko and co-workers recently reported a silicon-compatible broadband omnidirectional photodetector based on hierarchical ZnO/Si heterojunction.[16b] The device combined the excellent omnidirectional light absorption from honeycomb-structured silicon (H-Si) with the improved UV photosensitivity from ZnO nanowires (ZnO NWs). According to the 2D plots of UV–vis–NIR reflectance data of flat silicon (F-Si), H-Si, ZnO NWs/F-Si, and ZnO NWs/H-Si samples in Figure 3c, the reflectance of H-Si in the UV-to-NIR region is much lower than that of F-Si. The ZnO NWs/H-Si sample inherits the H-Si structure and exhibits an extremely low reflectance of ZnO NWs/H-Si sample in all the measured wavelength, contributing to the enhanced broadband photosensitivity. Furthermore, the ZnO NWs/H-Si device remained over 70% of the photocurrent even with a very high incident angle of 70°, while the remained photocurrent decreased to less than 40% in ZnO NWs/F-Si device. The omnidirectional property comes from the hexagonal holes that enable light absorptions at both the wall and the bottom of the honeycomb structure. According to the experimental results, larger hexagonal holes delivered stronger light absorption at high incident angles (>60°), and the minimal photocurrent variation was observed when the hole size was above 8.7 µm.

### 3.2. van der Waals Silicon Heterostructure

Traditional silicon-compatible heterojunction photodiodes have gained remarkable achievements in the enhanced optical detection at various wavelengths and omnidirectional photodetection. However, many of them suffer Auger combinations due to the lattice mismatch of the two composite materials and need special attentions to the interface structures[46] to satisfy the requirement of ultrafast photodetection. Fortunately, the rapid development of graphene has inspired the huge potential of 2D crystals. Many of these 2D crystals are endowed with excellent carrier conductivities. The most important 2D crystals, graphene, exhibit remarkable carrier mobilities of about $10^6$ cm$^2$ V$^{-1}$ s$^{-1}$ at low temperature,[47] and the typical 2D semiconductor, monolayer $MoS_2$, is reported with high carrier mobilities of about 100 cm$^2$ V$^{-1}$ s$^{-1}$ with an enhanced bandgap of 1.8 eV.[48] This has inspired a large number of novel photosensitive devices including vdW heterojunction devices.[49] Compared with traditional heterojunctions, atomically sharp 2D vdW heterostructures do not need to consider the lattice-match condition due to the weak interface bonding, offering fully compatibility with various amorphous or crystal substrates.[50] Thus, forming vdW heterojunctions with silicon has become a potential route to achieve ultrafast silicon-compatible photodetectors regardless of the lattice-match. Moreover, even a small depletion region can fully deplete the very thin photosensitive 2D crystals and guarantee high-speed photoresponse. A rich family of 2D crystals has been discovered, covering semimetals (graphenes[51] and 2D metals[52]), semiconductors (transition metal chalcogenides (TMDCs),[53] black phosphorus,[54]etc.), and insulators (hexagonal boron nitride[55] and layered oxides[56]). Such abundant material candidates have generated plenty of silicon-based vdW heterostructures to form Schottky junctions or heterojunctions.

Considering the much stronger inner layer bonding force than the interlayer vdW interaction, the vdW epitaxy on inert substrates has been developed as an important route to obtain 2D materials. For 2D crystals that are chemically inert to silicon, direct epitaxial fabrications are the most facile route to obtain vdW heterostructures with silicon substrates. The contact quality is also guaranteed in the epitaxial growth on thoroughly cleaned substrates. Many TMDCs are suitable for the epitaxial fabrication processes on silicon substrates, such as $MoS_2$,[57] $WSe_2$,[53c,58] and $Bi_2Se_3$.[26] In addition, the optical and electrical properties of these 2D crystals vary with the chemical composition and the material thickness, contributing to various epitaxial vdW heterostructures with flexible photoelectric properties. **Figure 4**a shows a typical silicon-compatible vdW heterojunction based on the epitaxial $MoS_2$.[24a] The Ar plasma–treated bare silicon substrate was dip-coated with Mo precursor film and got sulfured to finish the in situ fabrication of $MoS_2$ in sulfur vapor. A photodiode was constructed based on this n-$MoS_2$/n-silicon vdW heterojunction and showed excellent photosensitivity in the visible-near infrared region. The in situ epitaxial growth guaranteed high-quality vdW heterostructure and resulted in an ultrafast photoresponse with the capability to high-frequency light irradiation of about 100 kHz. Furthermore, the majority carrier transportation in the homotype n–n heterostructure contributed to an enhanced photogain and delivered a high responsivity of 11.9 A W$^{-1}$. The epitaxial $Bi_2Se_3$/silicon heterostructure is likewise endowed with high-performance photoresponse according to former reports. In Jie and co-workers' research (Figure 4b),[26] $Bi_2Se_3$ was epitaxially grown on prepatterned silicon to construct high-quality vdW photodiode. During the fabrication, $Bi_2Se_3$ powder was hot evaporated to provide the precursor vapor, and the [001]-oriented layered $Bi_2Se_3$ film was grown on the silicon substrate via vdW epitaxy. As a topological insulator, $Bi_2Se_3$ intrinsically forms a thin insulating interface on silicon and strongly diminishes the dark current, achieving a high detectivity of about $4.39 \times 10^{12}$ Jones. The build-in electric field from the vdW heterojunction effectively enhanced the charge separation efficiency and generated high light responsivity of 24.28 A W$^{-1}$. Moreover, the device perfectly displayed the superiority of epitaxial vdW heterostructures and delivered a remarkable response speed of $\tau_r/\tau_f = 2.5$ µs/5.5 µs.


© 2019 WILEY-VCH Verlag GmbH & Co. KGaA, Weinheim

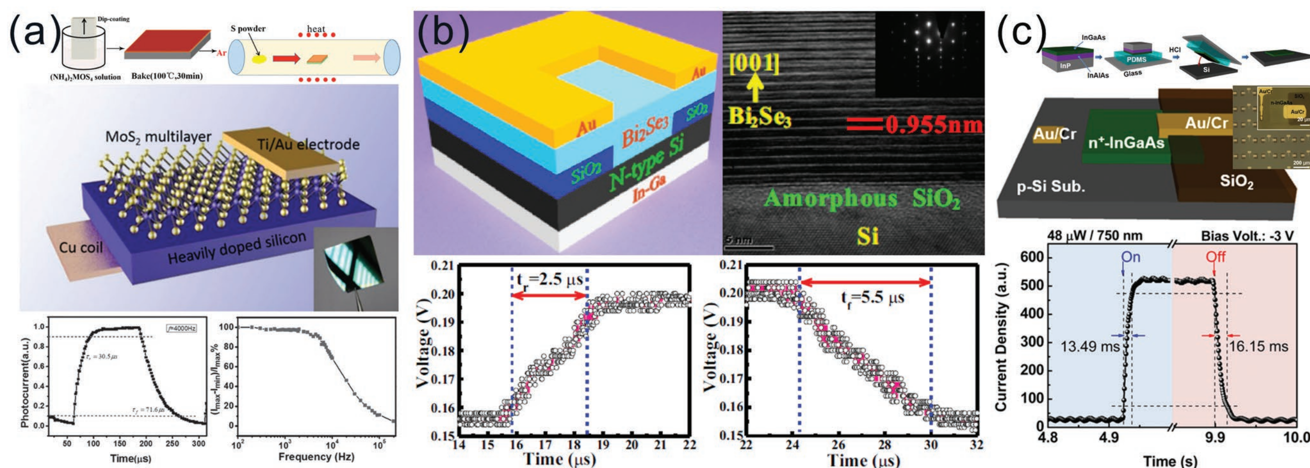


**Figure 4.** Silicon-compatible vdW heterojunction photodiodes avoiding lattice-match requirements: a) rapid silicon–$MoS_2$ photodiode based on epitaxially fabricated vdW heterostructure. Reproduced with permission.[24a] Copyright 2016, Wiley-VCH. b) Ultrafast silicon/$Bi_2Se_3$ photodiode based on vapor-based deposition. Reproduced with permission.[26] Copyright 2016, American Chemical Society. c) Delayed photoresponse in the nonepitaxially prepared silicon–InGaAs vdW heterojunction photodiode. Reproduced with permission.[20] Copyright 2016, American Chemical Society.

Although silicon epitaxial vdW heterostructures have huge advantages in ultrafast devices, many important 2D materials are incompatible with the epitaxial growth on silicon.[59] For example, the large-area fabrication of graphene is typically based on the chemical vapor deposition (CVD) on copper, nickel or gold foils.[51a,60] In addition to the vapor-based epitaxy, nonepitaxial synthesis methods such as exfoliations (mechanical, chemical, and electrochemical exfoliation) and solution-processed fabrications have produced various 2D crystals with different optical and electrical properties. These nonepitaxially synthesized 2D materials have effectively broadened the material candidates for silicon vdW heterostructures. Unlike the one-step epitaxial fabrication, the nonepitaxial construction of vdW heterostructures is usually composed of the following two steps: 1) the synthesis process of the object 2D materials through nonepitaxial methods or epitaxial growth on nonsilicon substrates; 2) the transfer process to attach the fabricated material to the silicon substrate. Figure 4c shows an example of nonepitaxially constructed vdW heterostructures.[20] First, the InAs/$n^+$-InGaAs/InAlAs stack structures were epitaxially grown on the InP substrate in a molecular beam epitaxy system, where InAs was the protective material and InAlAs was a lattice-matched buffer layer. Then the fabricated samples were attached to PDMS films and wet-etched to separate $n^+$-InGaAs membranes. The object InGaAs layer was finally transferred to p-Si to construct InGaAs/Si vdW heterojunction photodiodes. However, it is difficult to thoroughly avoid the air or solvent contamination in the transfer process, and nonepitaxial vdW heterostructures may contain considerable contact defects in the heterointerface. These interface defects may severely deteriorate the device properties and delay the response speed. Therefore, the aforementioned InGaAs/Si vdW device only delivered a moderate response speed with a rise/fall time of 13.49 ms/16.15 ms, and similar delays were also observed in other nonepitaxial vdW photodiodes. Unlike the ultrafast epitaxial vdW devices, the response speeds of nonepitaxial devices are often limited to millisecond level (e.g., reduced graphene oxide/n-Si heterojunction device with $\tau_r/\tau_f$ = 2 ms/3.7 ms[27]; graphene-silicon Schottky photodiode with $\tau_r/\tau_f$ = 0.32 ms/0.75 ms[28c]). Therefore, although the nonepitaxial construction enriches the material candidates and has contributed to many devices with various device bandwidths, the defective heterointerface may deprive the ultrafast photoresponse.

In brief summary, forming high-quality vdW heterostructures with various 2D materials has offered abundant flexibility to reduce the Auger loss in the junction interface and produce high-speed silicon-compatible devices. However, there are still some questions to fully guarantee the high performance. First, the introduced interface defects in no-epitaxial vdW heterostructures usually deteriorate the actual performances and special attentions should be paid to the contact quality to fully inherit the merits of vdW heterostructures. Moreover, the chemical stability and thermal resistance of many 2D semiconductors drop sharply as the thickness decreases to atomic level,[61] suffering a tradeoff between the material stability and the wanted bandgap increase from the quantum confinement effect.[62] Thus, the current vdW photodiodes mainly focus on low-bandwidth devices and further researches should keep on developing stable 2D semiconductors with higher bandgap for visible light or UV detections.

### 3.3. Lattice-Matched Silicon Heterojunction

Although forming high-quality vdW heterostructures with silicon offers to reduce the carrier loss in silicon-compatible photodiodes, the device bandwidths are still limited, as mentioned in Section 3.2. Thus, searching for proper materials to form lattice-matched heterojunctions with silicon is also an important route to suppress the Auger combinations and develop high-performance silicon-compatible devices. An ideal case to solve the lattice-match problems is to find suitable heterogeneous semiconductors with the same lattice structure and similar lattice parameter to that of silicon. Silicon is a typical member of group-IV semiconductor materials, and other group-IV semiconductors like germanium usually have the same lattice


© 2019 WILEY-VCH Verlag GmbH & Co. KGaA, Weinheim

structure but different lattice parameters. Forming controlled group-IV alloys may effectively adjust the lattice parameters and achieve excellent lattice-match with silicon, and considerable work has been done on this to find proper materials that are fully compatible with silicon industry. In Crespi and his coauthors research, group-IV direct-bandgap semiconductors were computationally designed to lattice-match silicon.[63] These works have inspired some promising materials for lattice-matched silicon-compatible photodiodes. However, the material candidates are still highly limited and their bandgaps are usually below 1.2 eV, setting barriers to visible light and UV detections.

Thanks to the controlled crystalline orientations in silicon materials, [100]-, [111]- or [110]-oriented silicon wafers could be facilely obtained, and the surface atom alignments on silicon substrates change with the crystal orientations. This provides additional choices for silicon lattice match and much more potential materials have emerged. For example, as a typical wide-bandgap p-type semiconductor, nickel oxide has been fully studied to form heterojunction photodiodes with various n-type semiconductors including n-Si.[64] However, although the p-NiO/n-Si heterojunctions in early studies effectively enhanced the UV photosensitivity of silicon,[64c] no lattice match was observed between NiO materials and the [100]-oriented silicon ($Si_{(100)}$) substrates. Recently, NiO nanoflakes was reported to have a rough alignment on [111]-oriented silicon ($Si_{(111)}$) wafers, and the fabricated vertical photodiode exhibited obviously enhanced photoelectric properties compared to former studies.[65] More systematically, Yang et al. reported the lattice match between trigonal selenium (t-Se) and $Si_{(111)}$, and proposed a vapor-based route to achieve aligned submicron Se crystals on silicon substrate (**Figure 5**).[19] They studied the lattice match between t-$Se_{(001)}$ and $Si_{(111)}$ through first-principles calculations using CASTEP.[66] The optimized structure is put in Figure 5a, where the lattice parameter of t-Se fits well with the atom spacing on $Si_{(111)}$ substrate. The lattice-matched Se-Si reduces the overall energy and diminishes the built-in electric field variation in the heterointerface (Figure 5b), strongly attenuating the Auger scattering effect near the p–n heterojunctions. In this way, the charge separation and charge collection are obviously facilitated and the prepared the Se/Si photodiode achieved the fastest response speed ($\tau_r + \tau_f \approx 1.975$ ms) (Figure 5c) among former Se-based photodetectors.[67] The response speed of the fabricated Se/Si photodiode is not only superior to other Se-based devices but also competitive to many recent similar-bandwidth photodetectors (e.g., $WS_2$/$CH_3NH_3PbI_3$ with $\tau_r/\tau_f \approx 2.7/7.5$ ms[68]; $MoS_2$/h-BN/graphene heterostructure with $\tau_r/\tau_f \approx 0.23/0.25$ s[50c]). The controlled n-typed doped silicon forms excellent energy band match with selenium and generates antibarriers on both conduction band and valence band. Thus, the Se/Si device delivered a similar wavelength cutoff to the selenium bandgap before the IR region, resulting in a high-speed UV-to-visible photoresponse with excellent sensitivity.

The lattice-matched silicon heterojunctions combine the photosensitive bandwidth of heterogeneous materials with fully enhanced photoresponse. This has generated some high-speed silicon-compatible photosensors with various photosensitive wavelengths, and an increasing number of material candidates are discovered. However, suitable materials are still highly hoped to make full use of the attractive merits. Seeking novel material candidates for lattice-matched silicon heterojunctions is still the main direction in the future.

As stated above, the photovoltaic photodetectors still attract a lot of attention and massive progresses have been made on silicon-compatible photodiodes. Apart from the traditional advantages in ultrafast photoresponse, enhanced properties have been achieved due to the developments of material fabrication. Various heterogeneous materials provide additional choices to extent the detection wavelength of silicon devices and even generate bias-tunable spectral response from the junction barrier. Heterojunction photodiodes often suffer delayed photoresponse due to the serious interface Auger combinations, but the van der Waals silicon heterostructures and the lattice-matched silicon heterojunctions have avoided this problem, thereby delivering high-performance photodiodes with ultrafast response.

## 4. Silicon-Compatible Photoconductive Devices

### 4.1. Silicon-Compatible Photoconductor and Photo-FETs

Apart from the photodiodes stated in Section 3, photoconductors are also one of the two most common photodetector types and have the potential to obtain higher responsivity than photodiodes. Unlike that in photodiodes, the

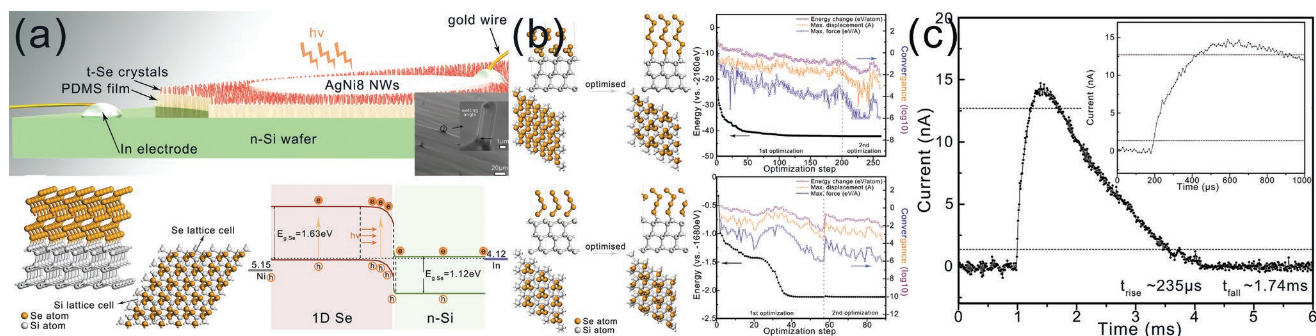


**Figure 5.** Silicon-compatible heterojunction photodiodes with silicon lattice match: a) the device structure of Se/Si photodiodes with lattice match and energy band match. b) First-principles optimizations of the Se/Si heterostructure. c) The fast response time of Se/Si photodiodes. Reproduced with permission.[19] Copyright 2018 American Chemical Society.


© 2019 WILEY-VCH Verlag GmbH & Co. KGaA, Weinheim

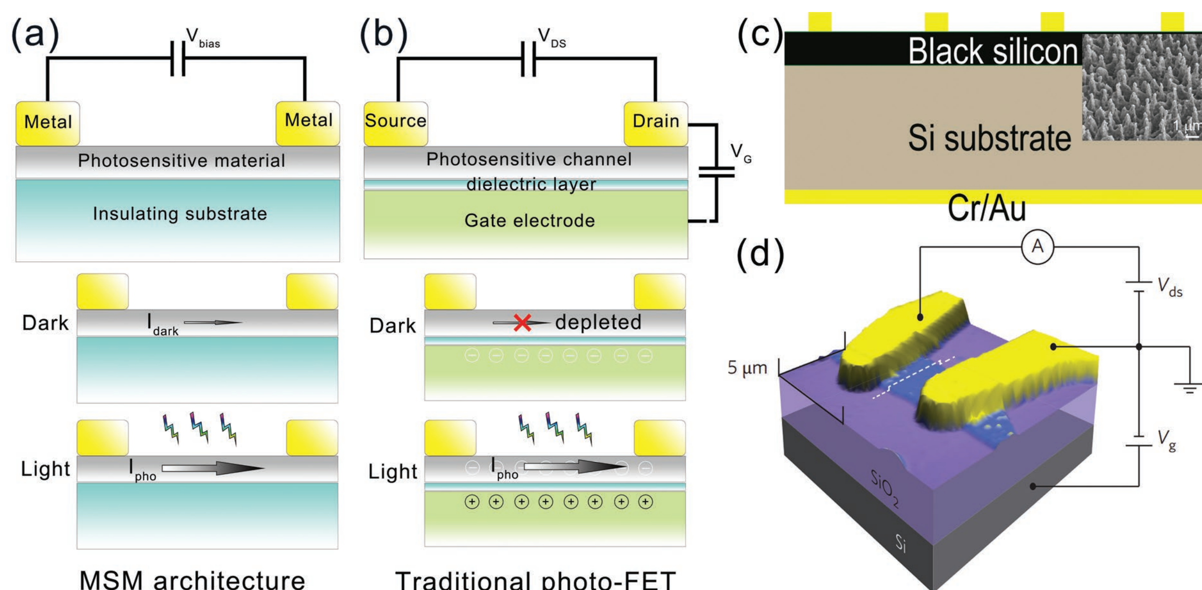


**Figure 6.** The device architectures and the working mechanisms of traditional photoconductive devices: a) MSM structure and b) photo-FET. The silicon-compatible photoconductive samples: c) a bulk-silicon based photoconductor with surface engineering as black silicon. Reproduced with permission.[73] Copyright 2016, IEEE. d) A typical field-effect transistor based on black phosphorus. Reproduced with permission.[74a] Copyright 2014, Springer Nature.

signal detection in photoconductors relies on the conductivity variations rather than the separated photogenerated carriers in the built-in electric field. The conductivity $\sigma$ of a material is determined by the carrier mobilities and the carrier concentrations as Equation (5)[69]

$$\sigma = nq\mu_n + pq\mu_p = (n_0 + \Delta n)q\mu_n + (p_0 + \Delta p)q\mu_p \tag{5}$$

where $n$ and $p$ are carrier concentrations for electrons and holes, respectively. $\mu_n$ and $\mu_p$ refer to the electron mobility and hole mobility, respectively, and $q$ is the electron charge. In a typical situation, the carrier mobility keeps constant for a given material and $\sigma$ depends on the carrier concentrations. When the incident light is induced, photoexcited carriers are generated and raise the carrier concentrations to provide extra conductivity. It is noteworthy that there are often considerable trapping states in semiconductor materials, where free carriers may drop in and get captured. The captured carriers have longer lifetime and can accumulate the whole carrier concentrations if only one type charge carriers are trapped and the other type keeps free. In this way, the trapping states introduce additional photoconductivity from the residual conductivity effect on the sacrifice of the response speed, which is also called the photoconductive gain. The photoconductive gain is typically evaluated by the gain ratio $G$, which is described as Equation (6)[70]

$$G = \frac{\tau_{trap}}{\tau_{drift}} = \frac{\tau_{trap}}{L_2}\mu V \tag{6}$$

where $\tau$ is the carrier lifetime, $L$ is the drifting distance of the free carriers, $\mu$ is the carrier mobility, and $V$ is the bias voltage.

The MSM structure is the simplest photoconductive architecture, which has been fully studied for photoconductive photodetectors.[71] In an MSM structured device, the photosensitive material forms a channel between two electrodes, and the photoconductivity is detected by the current variation under bias (**Figure 6**a). Generally, photosensitive materials with high carrier mobilities and direct bandgaps are preferred to achieve excellent photoconductive properties in an MSM device.[72] However, as the foundation of the semiconductor industry, silicon materials are indirect-bandgap material with weak photoconductive effects. Despite the excellent carrier mobility and the mature fabrications of silicon materials, the indirect bandgap severely decreases the photoconductivity of silicon. Although the absorption enhanced silicon materials like black silicon can effective increase the photoconductive current, as showed in Figure 6c, the photoelectric properties are still not so satisfying.[73] So silicon itself is typically unsuitable to act as high-performance photosensitive materials for photoconductive devices including MSM structures.

Although silicon can hardly act as goodish photoconductive materials due to the indirect bandgap, the facile dielectric epitaxy makes it excellent substrate for photo-FETs.[74] The photo-FET structures are proposed to decrease the dark current of the MSM devices and simultaneously inherit the photoconductive gain. The high photoconductive gain usually requires high-mobility photoconductive materials and high-quality Ohmic contact, and therefore the typical MSM device suffers a tradeoff between the responsivity and the sensitivity. Figure 6b displays the device structure of a photo-FET, where a gate electrode (usually heavily doped silicon) is vertically set to the MSM structure and electrically separated from the photoconductive channel by a thin epitaxial dielectric layer (typically $SiO_2$). The conductivity of the channel is modulated through the field-effect modulation, and simultaneously, light-induced charge carriers take the role of activating channel conductance. The field-effect


© 2019 WILEY-VCH Verlag GmbH & Co. KGaA, Weinheim

modulation comes from the gate voltage, which introduces a vertical electric field and depletes the photoconductive channel. The depleted channel delivers little lateral dark conductivity and limits the leakage current between the source and drain electrodes. When the incident light is induced, photoexcited carriers accumulate in the channel and generate similar photoelectric gains to that in MSM devices. In this way, photo-FETs inherit the high photoconductive gain and maintain low dark current at the same time. High-performance photo-FETs prefer thin channel materials with high mobility and large direct bandgap. Thin channels decrease the required gate voltage to get fully depleted. The high mobility guarantees high photoconductive gain and the large bandgap enables enough field-effect modulation.[70] The above-mentioned atomically thin 2D crystals in Section 3.2 can nearly possess all these preferred properties for channel materials, and numerous photo-FETs have been developed based on various 2D crystals like black phosphorus,[74a] $SnS_2$,[75] graphene,[3] and $MoS_2$[76] (Figure 6d). However, although thinner channel materials get depleted more easily and obtain lower leakage currents, the responsivity is also limited due to the decreased light absorption, setting a tradeoff between sensitivity and responsivity in photo-FETs. Moreover, the high mobility requires low defect density in the channel materials, which also reduces the trap states and decrease the photoconductive gain ratio.

### 4.2. Hybrid Photo-FETs

Considering the tradeoffs in traditional photo-FETs, Kufer et al. introduced the sensitizer layer above the channel materials to separate the carrier transportation and the light absorption. Here, we take their hybrid 2D–0D $MoS_2$–PbS quantum dot (QD) phototransistors as an example.[77] As showed in **Figure 7**a, colloidal p-type PbS QDs were utilized as the sensitizer and a hybrid FET was fabricated on a $Si/SiO_2$ substrate. The PbS QDs act as excellent absorption layer and the $MoS_2$ serves as high mobility thin channel. Unlike that in traditional photo-FETs, the photoinduced carriers generate in the high-absorption sensitizer layer and transport in the depleted channel (2D n-type $MoS_2$ (≥2 layers) here) due to the vertical gate voltage. The separated carrier transportation and light absorption enable individual modulation of the sensitizer and channel materials regardless of the aforementioned tradeoff between sensitivity and responsivity. The ultrathin 2D materials guarantee fully depleted channels and diminish the lateral leakage current in the dark through field-effect modulation, while the sensitizer offers high absorption to generate abundant photoinduced carriers. The built-in electric field drives the photoinduced carrier to the high-mobility channel and finally forms high photocurrent. Benefited from QDs' efficient light absorption and the high carrier mobility of $MoS_2$, high responsivity and low dark current were obtained when operated in the depletion mode. Therefore, the synergism of the hybrid structure provided a high photoconductive gain and the responsivity reached $10^5$–$10^6$ A $W^{-1}$. The shot noise determined detectivity reached $7 \times 10^{14}$ Jones under −100 V back-gate voltage due to the reduced dark current. The dark current could be further modulated by the back-gate voltage for higher sensitivity. These results show obvious superiority of the hybrid photo-FET structure. Moreover, the hybrid structure provides a universal route to improve the photoelectric performance and modulate the spectral response of photo-FETs. The carrier transportation is independent of the carrier mobility of the absorption layer and massive trap states are allowed in the sensitizer to achieve high photoconductive gain. The spectral response of the hybrid structure is actually determined by the bandgap of the sensitizer material, and tunable spectral response is offered by adjusting the absorption spectra of the sensitizer. Decorated with QDs with tunable absorption cutoff from the quantum confinement effect and material variations, the spectral response can be extended to the NIR region[78] regardless of the channel materials. The initiative of combining 2D crystal channels and colloidal QDs provides larger carrier multiplication

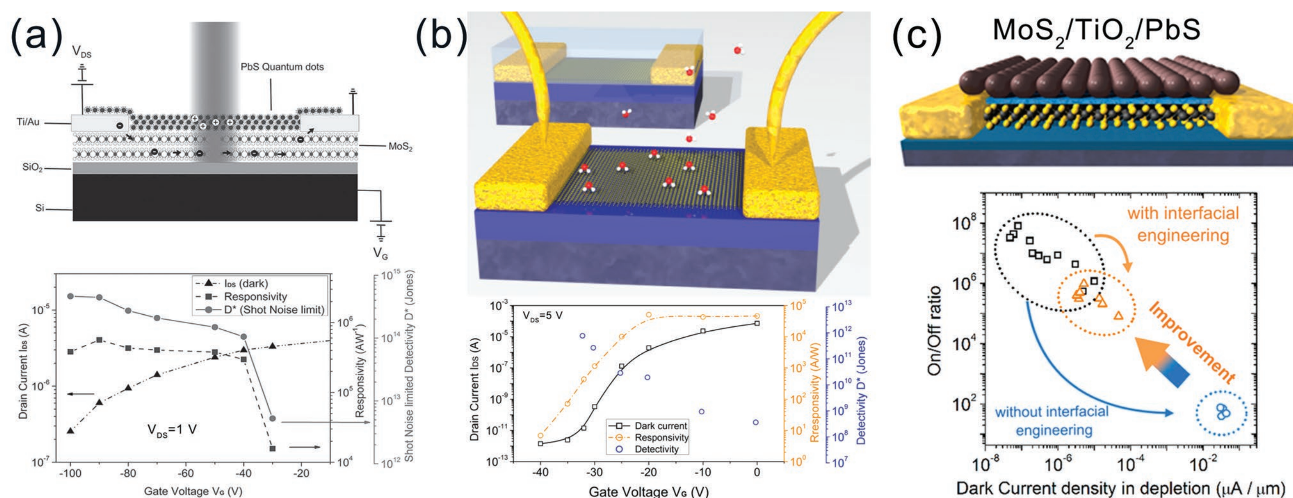


**Figure 7.** The reported hybrid photo-FETs combing high detectivity with photoconductive responsivity gain: a) hybrid 2D–0D $MoS_2$–PbS QDs phototransistor Reproduced with permission.[77] Copyright 2015, Wiley-VCH. b) $MoS_2$ photo-FET with n-type $HfO_2$ encapsulation as channel protection. Reproduced with permission.[82] Copyright 2015, American Chemical Society. c) Hybrid 2D–0D phototransistor with n-type $TiO_2$ interlayer as the interface passivation. Reproduced with permission.[83] Copyright 2016, American Chemical Society.

 © 2019 WILEY-VCH Verlag GmbH & Co. KGaA, Weinheim

and broader spectra absorption,[79] which paves the way in the quest to achieve high responsivity and low dark current in silicon-compatible photoconductive devices.

Ideally, ultrathin 2D semiconductors serve as excellent channel materials for high sensitivities in the aforementioned hybrid photo-FETs. However, atomically thin 2D crystals like monolayer and bilayer $MoS_2$ are highly sensitive to the environmental adsorbates owing to the extremely large surface to volume ratio. The environmental adsorbates introduce detrimental and uncontrollable effects to the optoelectrical properties and early FETs showed strong variations in their device performances. The adsorbate molecules such as $O_2$ and $H_2O$ introduce the photogating effect apart from the photoconductive effect,[80] which provides very long-lived charge trapping processes in the channel materials. The photogating effect may enhance the gain effect but usually dominates an extremely slow response speed, undermining the device performances.[81] Encapsulation offers a reasonable route to avoid the environmental adsorbate. Former research proved that the photogating effect is restrained and the whole photoelectric performances were improved through $HfO_2$ encapsulation, where $HfO_2$ not only isolated the FET channel from ambient air but also acted as strong n-type doping (Figure 7b).[82] Therefore, the encapsulation process also solved the drifting problem and significantly promoted the decay speed. Here, the $MoS_2/HfO_2$ device delivered a controllable responsivity of 10–$10^4$ A $W^{-1}$ and a response time ranging from ≈10 ms to 10 s. The transfer plots depicted that the on/off ratios of $MoS_2/HfO_2$ devices reached up to $10^8$. Taking predominant $1/f$-noise component into account, the device displayed a maximum measured value of $7.7 \times 10^{11}$ Jones at moderate gate voltage of −32 V, which was reported as the highest $MoS_2$ detectivity till then. The vanishing hysteresis presented in the modulation curve and strong n-type doping demonstrated that positive charges from the environmental adsorbates were removed, which mainly comes from the annealing process and the quenching of homopolar phonon modes from the dielectric screening. It was considered that the removed charge trapping adsorbates and the positively fixed charges which induced electrons into the channel gave further explanation for the strong n-type doping. By introducing this thin oxide protection, 2D crystal–based FETs achieved improved photoresponse with enhanced response speed.

Similarly, a thin $TiO_2$ interlayer was introduced to the $MoS_2$/PbS QD device to reduce the surface defects of the $MoS_2$ channel (Figure 7c). Although the QD sensitizer effectively combines high responsivity with high sensitivity, as stated above, QDs also introduce considerable surface defects to the $MoS_2$ channel. These surface defects act as dopants and trapping states, resulting in a reduced channel resistance and leading to the loss of high gate-tunable on/off ratios of pristine $MoS_2$. In order to solve the uncontrolled doping brought by the direct cross-linking of sensitizers at interlayer, a $TiO_2$ buffer layer was added between TMDCs and colloidal QDs to form well-aligned energy levels to passivate the defect sites.[83] The doping effect of $TiO_2$ layer is similar to that of the $HfO_2$ encapsulation. The doping compensation from the $MoS_2/TiO_2$ interface reduced the dark current to picoampere range. Additionally, the Fermi-level pinning from the large density of localized states in $MoS_2$ band gap could be intractable for the Ohmic contacts in low-dimensional semiconductors, and the $TiO_2$ buffer effective solved the contact problems. Compared with the device without $TiO_2$ layer, the on/off ratio increased two orders of magnitude. The $TiO_2$ interlayer not only suppressed the interface recombination from the hole injection into $MoS_2$, but also lowered the contact resistance and contributed to higher photoconductive gain. Thus, excellent charge separation and transportation resulted in an ultrahigh quantum efficiency of 28%. In terms of the sensitivity, the shot-noise limit detectivity was reported above $10^{14}$ Jones, and the experimentally determined detectivity was $5 \times 10^{12}$ Jones, which indicated further noise reduction in the future.

In summary, we discussed different silicon-compatible photoconductive photodetectors including silicon MSM photoconductors and silicon-compatible FETs. The intrinsic photoconductive effect of silicon is severely limited by the indirect bandgap even with obvious absorption enhancement, and the photoconductive response of silicon MSM devices almost reaches the ceiling. Fortunately, the facile dielectric epitaxy and doping make silicon materials excellent substrates for phototransistors, which is also compatible with the silicon IC technology. These silicon-compatible FETs suffer tradeoff between responsivity and sensitivity in the traditional structure, but the introduced sensitizers in hybrid FET structures effectively solved this problem by separating light absorption from the carrier transportation region. For a better comparison and comprehension, the typical reports of these device architectures are listed **Table 1**. The hybrid FET structures could be further optimized and have presented an unfolding propulsion for silicon compatible photodetectors with high responsivity, high responsivity as well as goodish response speed.

## 5. Photovoltage Field-Effect Transistors

As stated above in Section 4.1, photoconductive devices offer responsivity gains and the optimized photo-FETs combine high sensitivity with high responsivity. However, the responsivity gain of photoconductor and photo-FETs originates from the carrier trapping, and high gain value prefers a large lifetime $\tau_{trap}$ of the trapped carriers on the sacrifice of the response speed. Thus, the response time of these photo-FETs is typically limited to at least 1 ms (see Table 1). Although photodiodes have huger potential in high speed photodetection, the photovoltaic effect does not produce any responsivity gain. Therefore, traditional

**Table 1.** Typical reports of the hybrid photo-FETs.

| Architecture | Wavelength [nm] | $I_{dark}$ [A] | $R$ [A $W^{-1}$] | $\tau_f$ [s] | $D^*$ [Jones] | Ref. |
|---|---|---|---|---|---|---|
| $MoS_2$/PbS | 400–1500 | $2.6 \times 10^{-7}$<br>$V_G$ −100 V | $6 \times 10^5$ | 0.3–0.4 | $2 \times 10^{11}$ /$5 \times 10^{11}$ | [77] |
| $HfO_2/MoS_2$ | 550–800 | $\approx 10^{-12}$<br>$V_G$ −40 V | 10–$10^4$ | 0.01–10 | $7.7 \times 10^{11}$ | [82] |
| $MoS_2/TiO_2$/PbS | 600–1050 | – | $10^3$–$10^5$ | 0.012 | $5 \times 10^{12}$ | [83] |


© 2019 WILEY-VCH Verlag GmbH & Co. KGaA, Weinheim

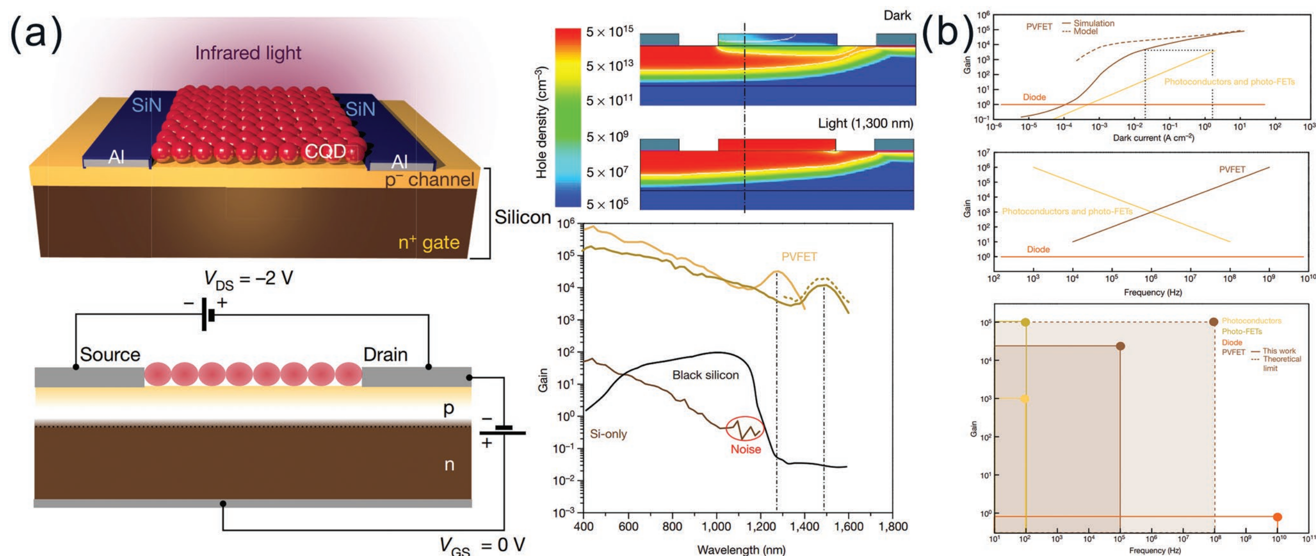


**Figure 8.** a) The silicon-compatible PVFET realizing ultrafast responsivity gain on the basis of the photovoltage and transconductance gain. b) The performance comparison among photodiodes, photoconductive devices and PVFETs. Reproduced with permission.[84] Copyright 2017, Springer Nature.

working mechanisms cannot meet the requirements of high response speed and high responsivity simultaneously.

The photovoltage and transconductance gain enables high responsivity and rapid responsivity at the same time,[69] which offers a solution for the speed limitation of photoconductive gain in high-frequency applications. Recently, Adinolfi and Sargent proposed and developed photovoltage field-effect transistors (PVFETs) and realized the photovoltage and transconductance gain in silicon-compatible architecture.[84] As displayed in **Figure 8**, the fabrication of PVFET devices is based on the commercial silicon techniques in today's chip industry. A heavily n-type doped silicon substrate is utilized as the bottom gate electrode and a lightly p-type doped silicon layer is epitaxially deposited on the $n^+$ silicon wafer as the channel material. The $p^-$ silicon channel is contacted with Ohmic source and drain electrodes and an n-type doped QD film is fabricated on the top of the silicon channel as the top photosensitive gate. The photosensitive gate is isolated from the source and drain and an insulating coat further prevents the electric contact. The surface traps in the Si/QD junction interface may strongly deteriorate the rectifying effect of the heterojunctions,[85] and special attentions should be paid on the passivation of surface traps to generate proper band alignment between QDs and the silicon channel. Owing to the top photosensitive gate and the heavily n-type doped bottom gate, the sandwiched $p^-$ silicon channel gets fully depleted and delivers high dark resistance at equilibrium. When the incident illumination turns on, photoinduced carriers are exclusively generated beyond the silicon channel in the photosensitive QD gate. The photoexcited carriers get separated in the Si/QD heterojunction, producing a photovoltaic voltage at the interface. The simulation results are displayed in Figure 8a, where the photoinduced bias effectively shrinks the depletion region and the photoinduced carriers are introduced to the silicon channel. Thereby the lateral conductivity of the channel switches on under the incident illumination, delivering a lateral photocurrent output at the source and drain bias ($V_{DS}$). The gate effect realizes high responsivity gain with high dark resistance while the gain value in the PVFET is related to the doping of the silicon channel. The photovoltage and transconductance gain in PVFETs is formulated as follows[84]

$$G = \frac{hv}{q} \times \frac{V_{ph} g_m}{P_{in}} \quad \text{and} \quad g_m = \frac{dI_{DS}}{dV_{ph}} \tag{7}$$

where $h$ refers to the Planck constant, $v$ is the light frequency, $q$ is the elemental charge, $V_{ph}$ is the photovoltage, $P_{in}$ is the incident photopower, $g_m$ is the transconductance, and $I_{DS}$ is the lateral drain–source current. Simulation results showed obvious gain advantages of the PVFET over photoconductors and photo-FETs under the same dark current requirement (Figure 8b).

Unlike the photoconductive gain, high gain value no longer requires large $\tau_{trap}$ at the cost of the response speed in PVFET. The total capacitance $C_{TOT}$ determines the operating frequency $f$ as $g_m/C_{TOT}$. Thus, high gain ratio is obtained in PVFET in high-frequency applications, resulting in an increasing responsivity as the response speed increases (Figure 8b). High photovoltage and transconductance gain actually leads to rapid photoresponse and thereby PVFET is endowed with remarkable device performance. The experimental corner frequency was reported as 100 kHz with a gain ratio of $10^4$–$10^6$ in the vis–NIR region under small $V_{DS}$ bias. The sandwiched depletion region effectively separates the carrier generation beyond the silicon channel even without bias voltage. Therefore, PVFET inherits the tunable spectral response of the photosensitive QD gate owing to the quantum confinement effect, which is very similar to that in the aforementioned 2D–0D hybrid photo-FETs. The Si/QD PVFET maintained excellent photoelectric performances beyond the absorption edge of silicon (>1500 nm) with high gain (>$10^4$), ultrafast response speed (100 kHz) and limited dark current of $10^{-1}$ to $10^1$A cm$^{-2}$. The device property could be further improved by utilizing advanced silicon processing to approach the theoretical limitation ($10^5$ gain at 100 mHz).


© 2019 WILEY-VCH Verlag GmbH & Co. KGaA, Weinheim

The architecture design of PVFET leverages a novel detection mechanism combining photovoltaic effect and photoconductive effect. The highly advanced performance benefits from the silicon techniques along with the developing colloidal QDs, leading a promising route to achieve ultrafast silicon-compatible photodetectors with high responsivity gain.

The emergence of photovoltaic field-effect transistors theoretically spearheads a novel direction for high-performance photodetectors combining excellent responsivity gain, high dark resistance and ultrafast response speed. However, the experimental results are still far from the theoretically simulation, which is possibly ascribed to the defect states in the QD–silicon interface. Defective QDs are necessary to obtain high absorption, while the defect states can also act as interface dopants into the silicon channel. Special interface treatments may effectively decrease the property deterioration.[86] Advanced silicon processing may further contribute to the enhancement of PVFETs.

## 6. Advances in Monolithic Photonic–Electronic System

### 6.1. Photonic–Electronic System on Traditional Silicon Chips

Silicon techniques on bulk single-crystal silicon materials have formed the foundation of today's integrated circuit chips, which still serves as the key component of most electronic platforms including photonic–electronic systems. The photonic–electronic systems combine photosensitive devices with electronic components to provide memory and logic functions for the incident signal, realizing smart photodetection for advanced applications. Communication is one of the most important applications of silicon-compatible photodetectors, where advanced logic functions are highly desired for signal treatments. Benefiting from the rapidly developing techniques, IR or even visible light communication has played important roles in short-distance IoT controlling, directly supporting the required data transmission. As for the long-distance microwave communication, IR photodetectors also act as the core component of microwave signal receivers, where radio-frequency (RF) signals are accepted and then treated. Nearly all the communication applications rely on the CMOS-based data processing, and the compatibility with CMOS effectively miniaturizes the structure. Moreover, the fully miniaturized optical communication has enabled in-chip data transmission to gradually replace the traditional electric connection, forming single-chip photonic–electronic microprocessor for the next-generation supercomputers. As stated in Sections 3, 4, 5, owing to the excellent carrier mobility as well as the facile doping and epitaxy, bulk single-crystal silicon materials have enabled plenty of high-performance photodetectors based on various device architectures and different working mechanisms. These advances have offered potential compatibility with current silicon chip electronics and inspired monolithic photonic–electronic systems with advanced properties

Most of former researches focused on the compatibility with bulk CMOS integrated circuits, which dominates the current chip industry. Early study integrated patterned ring-like silicon p–i–n photodiodes into small electronic circuits and developed small-sized electro-optic modulator that are suitable for further chip-scale integration.[87] The ring-like silicon resonant light-confining structure effectively enhances the light sensitivity and enables rapid photosensitivity to small refractive index changes of the silicon material. The total diameter of the modulator reached merely 12 µm then, and a number of studies have been reported to realize more complicated monolithic photonic–electronic networks based on similar silicon resonant light-confining structures.[88] Total silicon photonics like silicon homojunction photodiodes have excellent compatibility with silicon architectures and achieve high integration levels more easily, but the limited wavelength flexibility actually reduces the application. The weak IR photosensitivity of silicon homojunction device cannot satisfy the requirements of fiber-optic communication (1310 or 1550 nm). The introduction of heterogeneous photosensitive materials offers additional choices for silicon-compatible photonics,[89] which has enabled high-performance applications in communication field.[90] **Figure 9**a describes a typical optical channelizer slice using Si/Ge photodetector, which acts as a microwave signal receiver in radio-frequency communication.[91] The RF signals are captured by an antenna and the laser converts the signal to 1550 nm IR pulse. Then, the IR light is treated by the optical accessories to get split and filtered. The Si/Ge photodetector is directly integrated

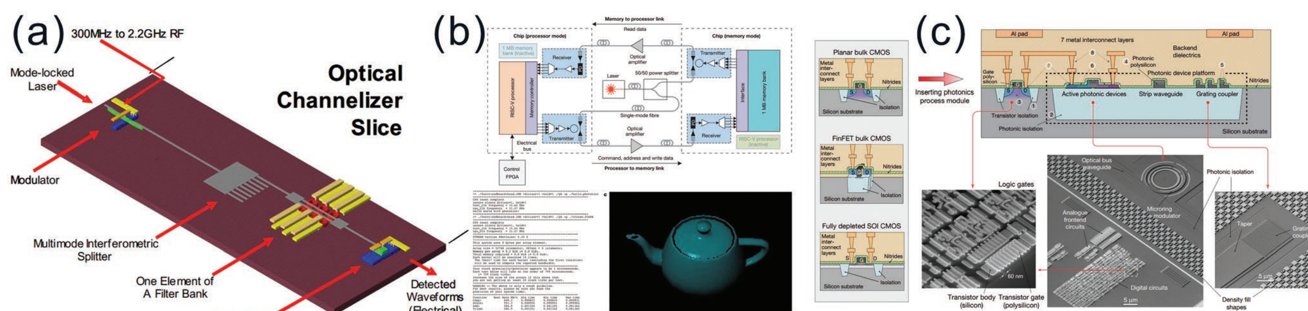


**Figure 9.** a) The description of a typical optical channelizer using Si-CMOS photodetectors for microwave signal receiving. Reproduced with permission.[91] Copyright 2006, The International Society for Optical Engineering. b) A monolithic photonic–electronic system serving as optical microprocessor using zero-change commercial 45 nm CMOS microelectronics foundry process. Reproduced with permission.[9] Copyright 2015, Springer Nature. c) A $SiO_2$ island–based integration strategy that is compatible with the leading CMOS techniques to provide superlarge-scale integrated photonic–electronic chips. Reproduced with permission.[95] Copyright 2018, Springer Nature.

 © 2019 WILEY-VCH Verlag GmbH & Co. KGaA, Weinheim

to a CMOS chip and they work together to electrically read out the incident information. These works have satisfied basic communication applications. However, the heterogeneous structure but complicates the large-scale integration to provide advanced logic functions in a custom process.[92] Therefore, early monolithic photonic–electronic systems[93] only contained a few photonics with simple circuits and complicated functions had to rely on external equipment.

Recently, Sun et al. directly adopted the commercial 45 nm complementary CMOS microelectronics foundry process to obtain a highly integrated single-chip electronic–photonic system with 850 photonic components and over 70 million transistors that work together to serve as a light-communication microprocessor (Figure 9b).[9] The light-communication system contains a dual-core RISC-V ISA microprocessor and a static random-access memory of 1 MB, providing the advanced logical operation and the signal memory, respectively. The photodetection component is based on waveguide-coupled FETs using silicon–germanium stressor, which has been reported to be directly compatible with the zero-change standard CMOS foundry.[94] In order to diminish the vertical current leakage, an etching treatment was developed to selectively remove the bottom silicon layer of the silicon-on-insulator (SOI) substrate within the photosensitive area. A receiver circuit was introduced to primarily resolve the photocurrent from the photodetectors and further logic calculation was accomplished in the microprocessor. Therefore, a direct chip-to-chip photocommunication was surprisingly realized and verified, indicating a potential route to break the limitation of electric connection and achieve more powerful computers.

### 6.2. Integrating Photonics with Advanced Silicon Nanoelectronics

Former monolithic photonic–electronic systems mostly relied on bulk SOI wafers, which serve as the traditional substrates of CMOS chips. Although traditional CMOS chips dominate the microprocessor architecture due to the abundant supply chain, the bulk silicon actually sets limitations to the superlarge-scale integration of photonic components into the chip technique. The biggest problem comes from the lack of the optical semiconductor materials in superlarge-scale integrations. The leading CMOS fabrication technologies like fin field effect transistor (Fin-FET) and thin-body fully depleted SOI (TBFD-SOI) pursue ultrathin etching process to achieve powerful integrated circuits, while too thin silicon materials are unable to support the photonic architectures, especially with the below 28 nm transistor nodes. An innovative route was proposed recently to fully resolve this problem, where thin film polycrystal-silicon photonics were stereoscopically fabricated on the ubiquitous $SiO_2$ island of CMOS chips and connected with metal interconnections (Figure 9c).[95] Thereby the photonic platform is integrated with a 65 nm CMOS process technology, which also suits the leading CMOS technologies (Fin-FET, TBFD-SOI, etc.). Additionally, this method offers potential monolithic photonic–electronic systems to get rid of the bulk SOI substrates. Massive low-cost large-area substrates such as transparent glass, metal foils or even flexible substrates are suitable for the integration as long as they are covered with a glass layer. Apart from the polycrystal silicon photonics, other thin-film photodetectors with glass substrates also become promising candidates to form monolithic photonic–electronic systems on a chip by this means, providing a universal integration strategy for the next-generation electronic–photonic platforms.

In brief summary, important studies have been reported to monolithically integrate photodetectors with electronic components, providing miniaturized single-chip photonic–electronic system with advanced logic and memory functions. Bulk CMOS chips still attract dominant attentions and zero-change commercial CMOS foundry process have been introduced to produce large-scale single-chip photonic–electronic systems with hundreds of photonics and millions of transistors. Additionally, the superlarge-scale photonic–electronic integration is enabled by a novel stereoscopic integration, which accommodates to the leading CMOS techniques as well as nonsilicon substrates. However, the integrated photodetectors in current reports are mainly traditional silicon photosensors with simple structures. In order to solve the integration problems with complicated silicon-compatible photodetectors, more attempts should be taken on both novel integration strategies and more silicon-compatible photodetectors that are directly compatible with the current IC technologies to achieve better properties.

## 7. Conclusion

As the foundational materials of the current semiconductor industry, bulk silicon has catalyzed powerful integrated circuits based on mature chip techniques like CMOS, forming the basis of smart equipment with advanced functions. Traditionally, photodetectors rely on external components to accomplish the signal memory and data analysis for smart photodetection. The introduction of additional circuits and external microprocessors causes considerable signal loss and seriously increases the size of the photonic–electronic system. As the development of IoT networks and the artificial intelligence, the oversized equipment no longer meets the requirements of smart sensors in modern miniaturized hardware. Developing photodetectors that are compatible with bulk silicon offers promising route to monolithically integrate photonics into silicon microchips, and many important progresses have been made to date. Numerous bulk silicon–based photodetectors have provided abundant candidates with various photoelectric properties to realize a photonic–electronic system on a chip as miniaturized smart photodetectors. As demonstrated in this review, plenty of significant advances have emerged in the device fabrication and the mechanism innovation of silicon-compatible devices. Silicon-compatible photodiodes inherit the merits of photovoltaic effect with rapid photoresponse and potential self-powered properties. Additionally, the material progresses in heterojunction silicon photodiodes have enabled sufficient spectral flexibility ranging from the UV-to-NIR region, where the junction barrier can even generate bias-tunable spectral response (typically in n–n or p–p hetero-photodiodes). Although the photoconductivity of silicon materials is limited due to the indirect bandgap, bulk silicon wafers serve as excellent substrates for photo-FETs. Former photo-FETs suffered tradeoff between low leakage current and


© 2019 WILEY-VCH Verlag GmbH & Co. KGaA, Weinheim

high photocurrent, while sensitizer-modified hybrid photo-FETs have successfully solved this problem by excluding the photocarrier generation region from the channel material. The advanced hybrid photo-FETs effectively maintain the enhanced responsivity from the photoconductive gain and obtain a low leakage current from the fully depleted channel, achieving remarkable high sensitivity with high responsivity. Traditional working mechanisms (photovoltaic effect and photoconductive effect) are not able to achieve high speed and high responsivity simultaneously. However, the emergence of silicon-compatible PVFET has successfully solved this problem based on photovoltage and transconductance gain. These advances have provided sufficient choices for the monolithic integration of photodetectors into electronic components.

Common fabrication methods like photolithography are sufficient to meet the requirements of simple photonic–electronic platforms with a few photonics and electronic circuits, which have gained some primary applications in advanced radar system and direct light sensing. More complicated photonic–electronic systems rely on higher integration levels and require advanced fabrication process. Fortunately, the zero-change commercial CMOS microelectronics foundry process is able to fit the integration requirements of monolithic photonic–electronic systems above the 45 nm geometries. Therefore, large-integration photonic–electronic microsystems have been developed with logic, memory, and interconnection functions. This enables a remarkable single-chip microprocessor that communicates directly using light and reveals a revolutionary future direction of powerful light-communication computers. Although the oversmall silicon regions in the leading ultrathin CMOS technologies like Fin-FET and TBFD-SOI are unable to support the photonic structures, a stereoscopic integration strategy has been proposed to achieve the monolithic integration of photonics with superlarge-scale integrated circuits. The stereoscopic integration strategy proposed and developed a universal route to utilize $SiO_2$ islands, which is ubiquitous in CMOS chips, as substrates for thin-film photonic structures. This integration strategy is not only fully compatible with the latest leading CMOS techniques but also suitable for various substrates such as metal, transparent glass, and flexible polymer film after coating $SiO_2$, making many nonsilicon-based photodetectors possible to form the next-generation monolithic photonic–electronic platforms.

Although massive researches have generally developed a complete system, challenges still exist to date. On the one hand, current silicon-compatible devices still have some shortcomings: the detection wavelength is typically limited to the UV-to-NIR region, and the device performances are far from the theoretical limits due to the interface quality and material defects. More work should be done to break the wavelength limitation and enhance the device fabrication. On the other hand, nearly all attempts in monolithic photonic–electronic integration are based on early silicon-compatible photodetectors with simple architectures such as silicon homojunction photodiodes and typical phototransistors. Although the fundamental problems have been solved, the integration of complicated silicon-compatible photodetector architectures with CMOS may lead to new technological problems. Moreover, the development of embedded systems and relevant control software on single-chip photonic–electronic systems may further upgrade the functions. Therefore, further researches and commercial studies are necessary to make full use of the developing silicon-compatible photodetectors. Despite the unsolved challenges, a bright future has been revealed to achieve fully advanced intelligent monolithic photonic–electronic systems with surprising applications, which may eventually lead the future life.

## Acknowledgements

This work was supported by the National Key Research and Development Program of China (Grant No. 2017YFA0204600), the National Natural Science Foundation of China (Grant Nos. 51721002, 51872050, 11674061, and 11811530065), Science and Technology Commission of Shanghai Municipality (Grant Nos. 18520744600, 18520710800, and 17520742400), and National Program for Support of Top-notch Young Professionals.

## Conflict of Interest

The authors declare no conflict of interest.

## Keywords

integration, photodetector, photonic–electronic, silicon-compatible

Received: November 19, 2018
Revised: January 11, 2019
Published online: February 25, 2019

[1] H. Chen, H. Liu, Z. Zhang, K. Hu, X. S. Fang, *Adv. Mater.* **2016**, *28*, 403.
[2] M. Y. Liao, L. Sang, T. Teraji, M. Imura, J. Alvarez, Y. Koide, *Jpn. J. Appl. Phys.* **2012**, *51*, 090115.
[3] a) I. Nikitskiy, S. Goossens, D. Kufer, T. Lasanta, G. Navickaite, F. H. Koppens, G. Konstantatos, *Nat. Commun.* **2016**, *7*, 11954; b) H. Chen, K. Liu, L. Hu, A. A. Al-Ghamdi, X. S. Fang, *Mater. Today* **2015**, *18*, 493.
[4] X. Xu, J. Chen, S. Cai, Z. Long, Y. Zhang, L. Su, S. He, C. Tang, P. Liu, H. Peng, X. S. Fang, *Adv. Mater.* **2018**, *30*, 1803165.
[5] Y. Dai, X. Wang, W. Peng, C. Xu, C. Wu, K. Dong, R. Liu, Z. L. Wang, *Adv. Mater.* **2018**, *30*, 1705893.
[6] a) C.-P. Lee, K.-Y. Lai, C.-A. Lin, C.-T. Li, K.-C. Ho, C.-I. Wu, S.-P. Lau, J.-H. He, *Nano Energy* **2017**, *36*, 260; b) Y.-H. Lin, S.-F. Lin, Y.-C. Chi, C.-L. Wu, C.-H. Cheng, W.-H. Tseng, J.-H. He, C.-I. Wu, C.-K. Lee, G.-R. Lin, *ACS Photonics* **2015**, *2*, 481.
[7] M. L. Tsai, M. Y. Li, J. R. D. Retamal, K. T. Lam, Y. C. Lin, K. Suenaga, L. J. Chen, G. Liang, L. J. Li, J. H. He, *Adv. Mater.* **2017**, *29*, 1701168.
[8] a) P. Ghelfi, F. Laghezza, F. Scotti, G. Serafino, A. Capria, S. Pinna, D. Onori, C. Porzi, M. Scaffardi, A. Malacarne, V. Vercesi, E. Lazzeri, F. Berizzi, A. Bogoni, *Nature* **2014**, *507*, 341; b) A. Motamedi, A. H. Nejadmalayeri, A. Khilo, C. W. Holzwarth, C. M. Soraceagaskar, E. P. Ippen, F. X. Kärtner, G. R. Zhou, H. I. Smith, H. J. O. E. Byun, *Opt. Express* **2012**, *20*, 4085.
[9] C. Sun, M. T. Wade, Y. Lee, J. S. Orcutt, L. Alloatti, M. S. Georgas, A. S. Waterman, J. M. Shainline, R. R. Avizienis, S. Lin, B. R. Moss, R. Kumar, F. Pavanello, A. H. Atabaki, H. M. Cook, A. J. Ou, J. C. Leu, Y. H. Chen, K. Asanovic, R. J. Ram, M. A. Popovic, V. M. Stojanovic, *Nature* **2015**, *528*, 534.


© 2019 WILEY-VCH Verlag GmbH & Co. KGaA, Weinheim

[10] S. Mudumba, S. de Alba, R. Romero, C. Cherwien, A. Wu, J. Wang, M. A. Gleeson, M. Iqbal, R. W. Burlingame, *J. Immunol. Methods* **2017**, *448*, 34.

[11] F. P. García de Arquer, A. Armin, P. Meredith, E. H. Sargent, *Nat. Rev. Mater.* **2017**, *2*, 16100.

[12] A. Rayes, S. Salam, *Internet of Things—From Hype to Reality*, Springer International Publishing, Cham, Switzerland **2017**.

[13] a) L. Su, W. Yang, J. Cai, H. Chen, X. S. Fang, *Small* **2017**, *13*, 1701687; b) J. Xu, W. Yang, H. Chen, L. Zheng, M. Hu, Y. Li, X. S. Fang, *J. Mater. Chem. C* **2018**, *6*, 3334; c) Y. Zhang, W. Xu, X. Xu, J. Cai, W. Yang, X. S. Fang, *J. Phys. Chem. Lett.* **2019**, *10*, 836; d) B. Zhao, F. Wang, H. Chen, L. Zheng, L. Su, D. Zhao, X. S. Fang, *Adv. Funct. Mater.* **2017**, *27*, 1700264; e) W. R. Wei, M. L. Tsai, S. T. Ho, S. H. Tai, C. R. Ho, S. H. Tsai, C. W. Liu, R. J. Chung, J. H. He, *Nano Lett.* **2013**, *13*, 3658; f) M. L. Tsai, D. S. Tsai, L. Tang, L. J. Chen, S. P. Lau, J. H. He, *ACS Nano* **2017**, *11*, 4564; g) H. P. Wang, A. C. Li, T. Y. Lin, J. H. He, *Nano Energy* **2016**, *23*, 1.

[14] H. P. Wang, J. H. He, *Adv. Energy Mater.* **2017**, *7*, 1602385.

[15] M. B. Johnston, *Nat. Photonics* **2017**, *11*, 268.

[16] a) Z. Wang, R. Yu, X. Wang, W. Wu, Z. L. Wang, *Adv. Mater.* **2016**, *28*, 6880; b) S. Lim, D.-S. Um, M. Ha, Q. Zhang, Y. Lee, Y. Lin, Z. Fan, H. Ko, *Nano Res.* **2017**, *10*, 22.

[17] a) T. Ji, Q. Liu, R. Zou, Y. Sun, K. Xu, L. Sang, M. Liao, Y. Koide, L. Yu, J. Hu, *Adv. Funct. Mater.* **2016**, *26*, 1400; b) T. Ji, Q. Liu, R. Zou, Y. Zhang, L. Wang, L. Sang, M. Liao, J. Hu, *J. Mater. Chem. C* **2017**, *5*, 12848.

[18] S. Chen, X. Liu, X. Qiao, X. Wan, K. Shehzad, X. Zhang, Y. Xu, X. Fan, *Small* **2017**, *13*, 1604033.

[19] W. Yang, K. Hu, F. Teng, J. Weng, Y. Zhang, X. S. Fang, *Nano Lett.* **2018**, *18*, 4697.

[20] D. S. Um, Y. Lee, S. Lim, J. Park, W. C. Yen, Y. L. Chueh, H. J. Kim, H. Ko, *ACS Appl. Mater. Interfaces* **2016**, *8*, 26105.

[21] Z. Liang, P. Zeng, P. Liu, C. Zhao, W. Xie, W. Mai, *ACS Appl. Mater. Interfaces* **2016**, *8*, 19158.

[22] Q. Hong, Y. Cao, J. Xu, H. Lu, J. He, J. L. Sun, *ACS Appl. Mater. Interfaces* **2014**, *6*, 20887.

[23] R. K. Chowdhury, R. Maiti, A. Ghorai, A. Midya, S. K. Ray, *Nanoscale* **2016**, *8*, 13429.

[24] a) Y. Zhang, Y. Yu, L. Mi, H. Wang, Z. Zhu, Q. Wu, Y. Zhang, Y. Jiang, *Small* **2016**, *12*, 1062; b) L. Wang, J. Jie, Z. Shao, Q. Zhang, X. Zhang, Y. Wang, Z. Sun, S.-T. Lee, *Adv. Funct. Mater.* **2015**, *25*, 2910.

[25] S. Gu, K. Ding, J. Pan, Z. Shao, J. Mao, X. Zhang, J. Jie, *J. Mater. Chem. A* **2017**, *5*, 11171.

[26] H. Zhang, X. Zhang, C. Liu, S.-T. Lee, J. Jie, *ACS Nano* **2016**, *10*, 5113.

[27] G. Li, L. Liu, G. Wu, W. Chen, S. Qin, Y. Wang, T. Zhang, *Small* **2016**, *12*, 5019.

[28] a) K. Huang, Y. Yan, K. Li, A. Khan, H. Zhang, X. Pi, X. Yu, D. Yang, *Adv. Opt. Mater.* **2018**, *6*, 1700793; b) X. Wan, Y. Xu, H. Guo, K. Shehzad, A. Ali, Y. Liu, J. Yang, D. Dai, C. T. Lin, L. Liu, *npj 2D Mater. Appl.* **2017**, *1*, 4; c) X. Li, M. Zhu, M. Du, Z. Lv, L. Zhang, Y. Li, Y. Yang, T. Yang, X. Li, K. Wang, H. Zhu, Y. Fang, *Small* **2016**, *12*, 595; d) A. Di Bartolomeo, F. Giubileo, G. Luongo, L. Iemmo, N. Martucciello, G. Niu, M. Fraschke, O. Skibitzki, T. Schroeder, G. Lupina, *2D Mater.* **2016**, *4*, 015024; e) T. Yu, F. Wang, Y. Xu, L. Ma, X. Pi, D. Yang, *Adv. Mater.* **2016**, *28*, 4912.

[29] M. Liu, F. P. de Arquer, Y. Li, X. Lan, G. H. Kim, O. Voznyy, L. K. Jagadamma, A. S. Abbas, S. Hoogland, Z. Lu, J. Y. Kim, A. Amassian, E. H. Sargent, *Adv. Mater.* **2016**, *28*, 4142.

[30] Z. Guo, D. Zhao, Y. Liu, D. Shen, J. Zhang, B. Li, *Appl. Phys. Lett.* **2008**, *93*, 163501.

[31] P. Yu, C.-H. Chang, C.-H. Chiu, C.-S. Yang, J.-C. Yu, H.-C. Kuo, S.-H. Hsu, Y.-C. Chang, *Adv. Mater.* **2009**, *21*, 1618.

[32] E. Garnett, P. Yang, *Nano Lett.* **2010**, *10*, 1082.

[33] a) M. Chen, B. Zhao, G. Hu, X. S. Fang, H. Wang, L. Wang, J. Luo, X. Han, X. Wang, C. Pan, Z. L. Wang, *Adv. Funct. Mater.* **2018**, *28*, 1706379; b) Z. Wang, R. Yu, C. Pan, Z. Li, J. Yang, F. Yi, Z. L. Wang, *Nat. Commun.* **2015**, *6*, 8401.

[34] Y. Liu, S. Niu, Q. Yang, B. D. Klein, Y. S. Zhou, Z. L. Wang, *Adv. Mater.* **2014**, *26*, 7209.

[35] Y. Gao, H. Cansizoglu, K. G. Polat, S. Ghandiparsi, A. Kaya, H. H. Mamtaz, A. S. Mayet, Y. Wang, X. Zhang, T. Yamada, E. P. Devine, A. F. Elrefaie, S.-Y. Wang, M. S. Islam, *Nat. Photonics* **2017**, *11*, 301.

[36] a) M. Ali, F. Zhou, K. Chen, C. Kotzur, C. Xiao, L. Bourgeois, X. Zhang, D. R. MacFarlane, *Nat. Commun.* **2016**, *7*, 11335; b) A. F. Halima, X. Zhang, D. R. MacFarlane, *Electrochim. Acta* **2017**, *235*, 453.

[37] a) P. Repo, A. Haarahiltunen, L. Sainiemi, M. Yli-Koski, H. Talvitie, M. C. Schubert, H. Savin, *IEEE J. Photovoltaics* **2013**, *3*, 90; b) M. Otto, M. Kroll, T. Kasebier, R. Salzer, *Appl. Phys. Lett.* **2012**, *100*, 191603.

[38] M. A. Juntunen, J. Heinonen, V. Vähänissi, P. Repo, D. Valluru, H. Savin, *Nat. Photonics* **2016**, *10*, 777.

[39] G. Dingemans, W. M. M. Kessels, *J. Vac. Sci. Technol., A* **2012**, *30*, 040802.

[40] a) H. C. Ko, M. P. Stoykovich, J. Song, V. Malyarchuk, W. M. Choi, C.-J. Yu, J. B. Geddes Iii, J. Xiao, S. Wang, Y. Huang, J. A. Rogers, *Nature* **2008**, *454*, 748; b) Y. M. Song, Y. Xie, V. Malyarchuk, J. Xiao, I. Jung, K.-J. Choi, Z. Liu, H. Park, C. Lu, R.-H. Kim, R. Li, K. B. Crozier, Y. Huang, J. A. Rogers, *Nature* **2013**, *497*, 95; c) K.-H. Jeong, J. Kim, L. P. Lee, *Science* **2006**, *312*, 557.

[41] H. Lin, F. Xiu, M. Fang, S. Yip, H. Y. Cheung, F. Wang, N. Han, K. S. Chan, C. Y. Wong, J. C. Ho, *ACS Nano* **2014**, *8*, 3752.

[42] Q. Lin, S. F. Leung, L. Lu, X. Chen, Z. Chen, H. Tang, W. Su, D. Li, Z. Fan, *ACS Nano* **2014**, *8*, 6484.

[43] a) C.-Y. Fang, Y.-L. Liu, Y.-C. Lee, H.-L. Chen, D.-H. Wan, C.-C. Yu, *Adv. Funct. Mater.* **2013**, *23*, 1412; b) X. Yan, D. J. Poxson, J. Cho, R. E. Welser, A. K. Sood, J. K. Kim, E. F. Schubert, *Adv. Funct. Mater.* **2013**, *23*, 583.

[44] K. Zhang, Y. H. Jung, S. Mikael, J.-H. Seo, M. Kim, H. Mi, H. Zhou, Z. Xia, W. Zhou, S. Gong, Z. Ma, *Nat. Commun.* **2017**, *8*, 1782.

[45] a) W. Q. Wu, H. L. Feng, H. S. Rao, Y. F. Xu, D. B. Kuang, C. Y. Su, *Nat. Commun.* **2014**, *5*, 3968; b) H. P. Wang, T. Y. Lin, C. W. Hsu, M. L. Tsai, C. H. Huang, W. R. Wei, M. Y. Huang, Y. J. Chien, P. C. Yang, C. W. Liu, *ACS Nano* **2013**, *7*, 9325.

[46] A. Jain, O. Voznyy, S. Hoogland, M. Korkusinski, P. Hawrylak, E. H. Sargent, *Nano Lett.* **2016**, *16*, 6491.

[47] A. S. Mayorov, D. C. Elias, I. S. Mukhin, S. V. Morozov, L. A. Ponomarenko, K. S. Novoselov, A. K. Geim, R. V. J. N. L. Gorbachev, *Nano Lett.* **2012**, *12*, 4629.

[48] B. Radisavljevic, A. Radenovic, J. Brivio, V. Giacometti, A. Kis, *Nat. Nanotechnol.* **2011**, *6*, 147.

[49] I. V. G. A. K. Geim, *Nature* **2013**, *499*, 419.

[50] a) F. X. Wang, *Nat. Mater.* **2015**, *14*, 264; b) Z. L. Deng, N. J. Conrad, H. Liu, Y. Gong, S. Najmaei, P. M. Ajayan, J. Lou, X. Xu, P. D. Ye, *ACS Nano* **2014**, *8*, 8292; c) Q. A. Vu, J. H. Lee, V. L. Nguyen, Y. S. Shin, S. C. Lim, K. Lee, J. Heo, S. Park, K. Kim, Y. H. Lee, W. J. Yu, *Nano Lett.* **2017**, *17*, 453.

[51] a) X. Li, W. Cai, J. An, S. Kim, J. Nah, D. Yang, R. Piner, A. Velamakanni, I. Jung, E. Tutuc, *Science* **2009**, *324*, 1312; b) Y. Hernandez, V. Nicolosi, M. Lotya, F. M. Blighe, Z. Sun, S. De, I. T. Mcgovern, B. Holland, M. Byrne, Y. K. Gun'Ko, *Nat. Nanotechnol.* **2008**, *3*, 563; c) D. Periyanagounder, P. Gnanasekar, P. Varadhan, J.-H. He, J. Kulandaivel, *J. Mater. Chem. C* **2018**, *6*, 9545.

[52] a) Z. Fan, X. Huang, Y. Han, M. Bosman, Q. Wang, Y. Zhu, Q. Liu, B. Li, Z. Zeng, J. Wu, *Nat. Commun.* **2015**, *6*, 6571; b) X. Huang,



© 2019 WILEY-VCH Verlag GmbH & Co. KGaA, Weinheim

S. Tang, X. Mu, Y. Dai, G. Chen, Z. Zhou, F. Ruan, Z. Yang, N. Zheng, *Nat. Nanotechnol.* **2011**, *6*, 28; c) H. Duan, N. Yan, R. Yu, C. R. Chang, G. Zhou, H. S. Hu, H. Rong, Z. Niu, J. Mao, H. Asakura, *Nat. Commun.* **2014**, *5*, 3093.

[53] a) C. Tan, H. Zhang, *Nat. Commun.* **2015**, *6*, 7873; b) Y. Shi, H. Li, L. J. Li, *Chem. Soc. Rev.* **2015**, *44*, 2744; c) T. Yang, B. Zheng, Z. Wang, T. Xu, C. Pan, J. Zou, X. Zhang, Z. Qi, H. Liu, Y. Feng, W. Hu, F. Miao, L. Sun, X. Duan, A. Pan, *Nat. Commun.* **2017**, *8*, 1906.

[54] A. Castellanosgomez, L. Vicarelli, E. Prada, J. O. Island, K. L. Narasimhaacharya, S. I. Blanter, D. J. Groenendijk, M. Buscema, G. A. Steele, J. V. Alvarez, *2D Mater.* **2014**, *1*, 025001.

[55] G. Kim, A. R. Jang, H. Y. Jeong, Z. Lee, D. J. Kang, H. S. Shin, *Nano Lett.* **2013**, *13*, 1834.

[56] M. Osada, T. Sasaki, *Adv. Mater.* **2012**, *24*, 210.

[57] Y. H. Lee, X. Q. Zhang, W. Zhang, M. T. Chang, C. T. Lin, K. D. Chang, Y. C. Yu, J. T. Wang, C. S. Chang, L. J. Li, T. W. Lin, *Adv. Mater.* **2012**, *24*, 2320.

[58] Z.-Q. Xu, Y. Zhang, Z. Wang, Y. Shen, W. Huang, X. Xia, W. Yu, Y. Xue, L. Sun, C. Zheng, Y. Lu, L. Liao, Q. Bao, *2D Mater.* **2016**, *3*, 041001.

[59] R. Dong, T. Zhang, X. Feng, *Chem. Rev.* **2018**, *118*, 6189.

[60] a) K. S. Kim, Y. Zhao, H. Jang, S. Y. Lee, J. M. Kim, K. S. Kim, J. H. Ahn, P. Kim, J. Y. Choi, B. H. Hong, *Nature* **2009**, *457*, 706; b) Y. Zhang, L. Zhang, C. Zhou, *Acc. Chem. Res.* **2013**, *46*, 2329.

[61] A. Castellanos-Gomez, *J. Phys. Chem. Lett.* **2015**, *6*, 4280.

[62] L. Brus, *J. Phys. Chem.* **1986**, *90*, 2555.

[63] P. Zhang, V. H. Crespi, E. Chang, S. G. Louie, M. L. Cohen, *Nature* **2001**, *409*, 69.

[64] a) L. Zheng, F. Teng, Z. Zhang, B. Zhao, X. S. Fang, *J. Mater. Chem. C* **2016**, *4*, 10032; b) F. Teng, K. Hu, W. Ouyang, X. S. Fang, *Adv. Mater.* **2018**, *30*, 1706262; c) J.-M. Choi, S. Im, *Appl. Surf. Sci.* **2005**, *244*, 435; d) X. S. Fang, L. F. Hu, K. F. Huo, B. Gao, L. J. Zhao, M. Y. Liao, P. K. Chu, Y. Bando, D. Golberg, *Adv. Funct. Mater.* **2011**, *21*, 3907.

[65] Y. Zhang, T. Ji, W. Zhang, G. Guan, Q. Ren, K. Xu, X. Huang, R. Zou, J. Hu, *J. Mater. Chem. C* **2017**, *5*, 12520.

[66] S. J. Clark, M. D. Segall, C. J. Pickard, P. J. Hasnip, M. I. J. Probert, K. Refson, M. C. Payne, *Z. Kristallogr. – Cryst. Mater.* **2005**, *220*, 567.

[67] a) K. Hu, H. Chen, M. Jiang, F. Teng, L. Zheng, X. S. Fang, *Adv. Funct. Mater.* **2016**, *26*, 6641; b) P. Yu, K. Hu, H. Chen, L. Zheng, X. S. Fang, *Adv. Funct. Mater.* **2017**, *27*, 1703166; c) L. Zheng, K. Hu, F. Teng, X. S. Fang, *Small* **2017**, *13*, 1602448; d) K. Hu, F. Teng, L. Zheng, P. Yu, Z. Zhang, H. Chen, X. S. Fang, *Laser Photonics Rev.* **2017**, *11*, 1600257.

[68] C. Ma, Y. Shi, W. Hu, M. H. Chiu, Z. Liu, A. Bera, F. Li, H. Wang, L. J. Li, T. Wu, *Adv. Mater.* **2016**, *28*, 3683.

[69] S. M. Sze, K. K. Ng, *Physics of Semiconductor Devices*, 3rd ed., Wiley-Blackwell, Hoboken, NJ **2007**.

[70] D. Kufer, G. Konstantatos, *ACS Photonics* **2016**, *3*, 2197.

[71] a) S. Liu, L. Hu, X. Xu, A. A. Al-Ghamdi, X. S. Fang, *Small* **2015**, *11*, 4267; b) Z. M. Zhang, Y. Ning, X. S. Fang, *J. Mater. Chem. C* **2019**, *7*, 223; c) X. Xu, S. Li, J. Chen, S. Cai, Z. Long, X. S. Fang, *Adv. Funct. Mater.* **2018**, *28*, 1802029.

[72] D. S. Tsai, C. A. Lin, W. C. Lien, H. C. Chang, Y. L. Wang, J. H. He, *ACS Nano* **2011**, *5*, 7748.

[73] X. Y. Yu, Z. H. Lv, C. H. Li, X. Han, J. H. Zhao, *IEEE Sens. J.* **2016**, *16*, 5227.

[74] a) L. Li, Y. Yu, G. J. Ye, Q. Ge, X. Ou, H. Wu, D. Feng, X. H. Chen, Y. Zhang, *Nat. Nanotechnol.* **2014**, *9*, 372; b) Y. Zhang, D. J. Hellebusch, N. D. Bronstein, C. Ko, D. F. Ogletree, M. Salmeron, A. P. Alivisatos, *Nat. Commun.* **2016**, *7*, 11924; c) X. Yu, T. J. Marks, A. Facchetti, *Nat. Mater.* **2016**, *15*, 383; d) Y. Wen, L. Yin, P. He, Z. Wang, X. Zhang, Q. Wang, T. A. Shifa, K. Xu, F. Wang, X. Zhan, F. Wang, C. Jiang, J. He, *Nano Lett.* **2016**, *16*, 6437; e) D. H. Kang, S. R. Pae, J. Shim, G. Yoo, J. Jeon, J. W. Leem, J. S. Yu, S. Lee, B. Shin, J. H. Park, *Adv. Mater.* **2016**, *28*, 7799.

[75] X. Zhou, Q. Zhang, L. Gan, H. Li, T. Zhai, *Adv. Funct. Mater.* **2016**, *26*, 4405.

[76] S. B. Desai, S. R. Madhvapathy, A. B. Sachid, J. P. Llinas, Q. Wang, G. H. Ahn, G. Pitner, M. J. Kim, J. Bokor, C. Hu, H.-S. P. Wong, A. Javey, *Nature* **2016**, *354*, 99.

[77] D. Kufer, I. Nikitskiy, T. Lasanta, G. Navickaite, F. H. Koppens, G. Konstantatos, *Adv. Mater.* **2015**, *27*, 176.

[78] B. Sun, O. Voznyy, H. Tan, P. Stadler, M. Liu, G. Walters, A. H. Proppe, M. Liu, J. Fan, T. Zhuang, J. Li, M. Wei, J. Xu, Y. Kim, S. Hoogland, E. H. Sargent, *Adv. Mater.* **2017**, *29*, 1700749.

[79] R. Saran, R. J. Curry, *Nat. Photonics* **2016**, *10*, 81.

[80] M. M. Furchi, D. K. Polyushkin, A. Pospischil, T. Mueller, *Nano Lett.* **2014**, *14*, 6165.

[81] S. Tongay, J. Zhou, C. Ataca, J. Liu, J. S. Kang, T. S. Matthews, L. You, J. Li, J. C. Grossman, J. Wu, *Nano Lett.* **2013**, *13*, 2831.

[82] D. Kufer, G. Konstantatos, *Nano Lett.* **2015**, *15*, 7307.

[83] D. Kufer, T. Lasanta, M. Bernechea, F. H. L. Koppens, G. Konstantatos, *ACS Photonics* **2016**, *3*, 1324.

[84] V. Adinolfi, E. H. Sargent, *Nature* **2017**, *542*, 324.

[85] S. Masala, V. Adinolfi, J. P. Sun, S. Del Gobbo, O. Voznyy, I. J. Kramer, I. G. Hill, E. H. Sargent, *Adv. Mater.* **2015**, *27*, 7445.

[86] a) Y. Hou, X. Du, S. Scheiner, D. P. McMeekin, Z. Wang, N. Li, M. S. Killian, H. Chen, M. Richter, I. Levchuk, N. Schrenker, E. Spiecker, T. Stubhan, N. A. Luechinger, A. Hirsch, P. Schmuki, H.-P. Steinrück, R. H. Fink, M. Halik, H. J. Snaith, C. J. Brabec, *Science* **2017**, *358*, 1192; b) J. Choi, Y. Kim, J. W. Jo, J. Kim, B. Sun, G. Walters, F. P. Garcia de Arquer, R. Quintero-Bermudez, Y. Li, C. S. Tan, L. N. Quan, A. P. T. Kam, S. Hoogland, Z. Lu, O. Voznyy, E. H. Sargent, *Adv. Mater.* **2017**, *29*, 1702350.

[87] Q. Xu, B. Schmidt, S. Pradhan, M. Lipson, *Nature* **2005**, *435*, 325.

[88] a) C. Batten, A. Joshi, F. X. Kärtner, R. J. Ram, V. Stojanović, K. Asanović, J. Orcutt, A. Khilo, B. Moss, C. W. J. I. M. Holzwarth, *IEEE Micro* **2009**, *29*, 8; b) A. Shacham, K. Bergman, L. P. Carloni, *IEEE Trans. Comput.* **2008**, *57*, 1246; c) S. Beamer, C. Sun, Y. J. Kwon, A. Joshi, C. Batten, in *ACM SIGARCH Computer Architecture News*, Vol. *38*, **2010**, ACM, New York p. 129.

[89] J. Capmany, D. Novak, *Nat. Photonics* **2007**, *1*, 319.

[90] G. Kim, H. Park, J. Joo, K. S. Jang, M. J. Kwack, S. Kim, I. G. Kim, J. H. Oh, S. A. Kim, J. Park, S. Kim, *Sci. Rep.* **2015**, *5*, 11329.

[91] J. A. Kubby, L. C. Kimerling, G. T. Reed, D. Ahn, A. B. Apsel, M. Beals, D. Carothers, Y. K. Chen, T. Conway, D. M. Gill, M. Grove, C. Y. Hong, M. Lipson, J. Liu, J. Michel, D. Pan, S. S. Patel, A. T. Pomerene, M. Rasras, D. K. Sparacin, K. Y. Tu, A. E. White, C. W. Wong, *Proc. SPIE* **2006**, *6125*, 612502.

[92] N. Dupuis, B. Lee, J. Proesel, A. V. Rylyakov, R. Rimolo-Donadio, C. W. Baks, C. L. Schow, A. Ramaswamy, J. E. Roth, R. S. Guzzon, B. Koch, D. K. Sparacin, G. A. Fish, presented at *Optical Fiber Communication Conference*, Optical Society of America, San Francisco, CA March **2014**.

[93] a) J. F. Buckwalter, X. Zheng, G. Li, K. Raj, A. V. J. I. J. o. S.-S. C. Krishnamoorthy, *IEEE J. Solid-State Circuits* **2012**, *47*, 1309; b) W. M. J. Green, S. Assefa, A. Rylyakov, C. Schow, F. Horst, Y. A. Vlasov, presented at *Adv. Photonics*, Toronto, June **2011**.

[94] L. Alloatti, S. A. Srinivasan, J. S. Orcutt, R. J. R. J. A. P. Letters, *Appl. Phys. Lett.* **2015**, *107*, 041104.

[95] A. H. Atabaki, S. Moazeni, F. Pavanello, H. Gevorgyan, J. Notaros, L. Alloatti, M. T. Wade, C. Sun, S. A. Kruger, H. Meng, K. Al Qubaisi, I. Wang, B. Zhang, A. Khilo, C. V. Baiocco, M. A. Popovic, V. M. Stojanovic, R. J. Ram, *Nature* **2018**, *556*, 349.


© 2019 WILEY-VCH Verlag GmbH & Co. KGaA, Weinheim